ESCAP/WMO
Typhoon Committee

Available online at www.sciencedirect.com

ScienceDirect

Tropical Cyclone Research and Review 12 (2023) 10–29

www.keaipublishing.com/tcrr

Research advances on internal processes affecting tropical cyclone intensity change from 2018–2022

Xiaomin Chen [a,b,*,1], Christopher M. Rozoff [c,*], Robert F. Rogers [a], Kristen L. Corbosiero [d], Dandan Tao [e], Jian-Feng Gu [f,g], Falko Judt [c], Eric A. Hendricks [c], Yuqing Wang [h], Michael M. Bell [i], Daniel P. Stern [j], Kate D. Musgrave [i], John A. Knaff [k], John Kaplan [a]

[a] *NOAA/OAR/Atlantic Oceanographic and Meteorological Laboratory, Miami, USA*
[b] *University of Alabama in Huntsville, Huntsville, USA*
[c] *National Center for Atmospheric Research, Boulder, USA*
[d] *University at Albany/State University of New York, Albany, USA*
[e] *University of Bergen, Bergen, Norway*
[f] *Nanjing University, Nanjing, China*
[g] *University of Reading, Reading, UK*
[h] *University of Hawaii at Manoa, Honolulu, USA*
[i] *Colorado State University, Fort Collins, USA*
[j] *University Corporation for Atmospheric Research, Monterey, USA*
[k] *NOAA Center for Satellite Applications and Research, Fort Collins, USA*

Available online 8 May 2023

Abstract

This contribution summarizes the significant progress in a variety of topic areas related to internal tropical cyclone (TC) intensity change processes over 2018–2022 from the WMO Tenth International Workshop on Tropical Cyclones (IWTC-10). These topic areas include surface and boundary layer processes; TC internal structure and microphysical processes; and, radiation interactions with TCs. Recent studies better frame the uncertainty in the surface drag and enthalpy coefficients at high wind speeds. These parameters greatly impact TC intensity and it is therefore important that more direct measurements of these boundary layer parameters are made. Particularly significant scientific strides have been made in TC boundary layers. These advancements have been achieved through improved coupled models, large-eddy simulations, theoretical advancements, and detailed observations. It is now clear that the research field needs to better represent the eddy viscosity throughout the depth of the boundary layer. Furthermore, detailed study of coherent structures in TC boundary layers will likely be a propitious direction for the research community. Meanwhile, in-depth observational field campaigns and assiduous data analysis have made significant headway into verifying theory and modeling studies of intensification processes related to TC vortex alignment, efficient latent heating distributions, and overall 3D structure. Substantial efforts have also been made to better understand the intricate roles radiative processes play in TC evolution and intensity change. Finally, some promising progress has been made in the development of time-dependent theories of TC intensification and the predictability of internal TC intensity change. Overall, there have been well-earned gains in the understanding of intensity change processes intrinsic to the TC

* Corresponding authors.
E-mail addresses: xc0011@uah.edu (X. Chen), rozoff@ucar.edu (C.M. Rozoff).
Peer review under responsibility of Shanghai Typhoon Institute of China Meteorological Administration.
[1] Current affiliation: Department of Atmospheric and Earth Science, University of Alabama in Huntsville, Huntsville, USA.

ELSEVIER Production and Hosting by Elsevier on behalf of KeAi

https://doi.org/10.1016/j.tcrr.2023.05.001

system, but the journey is not complete. This paper highlights some of the most relevant and important research areas that are still shedding new light into internal factors governing TC intensity change.

Keywords: Tropical cyclone; Intensity; Internal dynamics; Boundary-layer processes; Observations; Predictability

1. Introduction

Tropical cyclones (TCs, see a full list of acronyms in Table 1) have long captivated the scientific community in view of the fact that these organized weather systems are products of their environment, beholden to the large-scale characteristics of the sea, land, and atmosphere, and yet, throughout their lifespans, these storms create a breathtaking array of internal dynamics. Internal TC dynamics range from the intricate organization of boundary layer turbulence, imposing violent conditions at the sea surface that thereby impact surface layer fluxes driving the storm, to convective elements that, in mature storms, become structurally arranged from circular, striated eyewalls in the innermost TC region to spiraling convective-stratiform rainbands that sometimes behave semi-autonomously in a storm's outer expanses. Spatial patterns of heating and cooling emanating from microphysical and radiation processes are of fundamental importance to a TC's structure and evolution. Intense 3D wind shears and strong thermodynamic gradients in the inner core of mature TCs unleash a variety of instabilities, such as boundary layer rolls and eyewall asymmetries, which can modify the trajectory of a storm's intensity. The multiscale nature of TCs enables rapid two-way cascades of energy between the microscale and large-scale atmosphere. These complex and fascinating aspects of TCs continue to both challenge and motivate the research and forecasting communities.

In the following sections, we summarize the vital research studies conducted over the past four years in the area of internal TC dynamics. We emphasize one cannot fully describe TC intensity change without considering the interactions between environmental conditions imposed on a TC and the internal dynamics that are impacted by and modify the environment. This review focuses solely on internal TC dynamics, including some of the dynamics set into motion by environmental stimuli. The rest of this paper is organized as follows. In section 2, we cover the topics of the TC's lower boundary condition (including air-sea interaction), the boundary layer, microphysics, radiation, the capacious topic of internal vortex-convective structure and dynamics, and finally recent theoretical and empirical advances in the area of TC intensification rate. Section 3 connects aspects of storm internal dynamics to the subject of intensity change theory and predictability. Guided by the current state of knowledge, the final section suggests the most auspicious avenues of inquiry in the forthcoming years.

2. Physical processes related to intensity change

2.1. Surface fluxes and other lower boundary condition considerations

a) Update on C_d/C_k Knowledge

Exchange coefficients for enthalpy (C_k) and momentum (C_d) are known to affect the intensity of TCs. Obtaining accurate values of C_k and C_d in hurricane conditions remains a priority in the TC community. Unfortunately, the uncertainty in these exchange coefficients remains large, especially in high winds. The nonlinear impacts of C_k and C_d on the modeled TC intensity and the ocean coupling were reported by Nystrom et al. (2020).

Laboratory measurements from Komori et al. (2018) and Troitskaya et al. (2018) showed a sharp increase of C_k at wind

Table 1
Acronyms used in this paper.

ACT	electrically active
CISK	Conditional Instability of the Second Kind
ERCs	eyewall replacement cycles
INACT	inactive
KPP	*K*-profile parameterizations
LLC	low-level circulation
LES	large-eddy simulations
MLC	midlevel circulation
MPI	Maximum Potential Intensity
MYNN	Mellor–Yamada–Nakanishi–Niino
NOAA	National Oceanic and Atmospheric Administration
NWP	numerical weather prediction
PBL	planetary boundary layer
PIR	potential intensification rate
QUASI	quasi-electrically active
RCE	radiative-convective equilibrium
RI	rapid intensification
RMW	radius of maximum wind
SEF	secondary eyewall formation
SFX	surface enthalpy flux
SHIPS	Statistical Hurricane Intensity Prediction Scheme
SST	sea surface temperature
sUAS	sUAS – small unmanned aircraft systems
TC	tropical cyclone
TKE	turbulence kinetic energy
VWS	vertical wind shear
WISHE	Wind-Induced Surface Heat Exchange
WWLLN	World Wide Lightning Location Network

speeds ≥35 m s^{-1} and, thus, C_k values in high-wind conditions are much greater than earlier findings. They attributed the noticeable increase in C_k at high wind speeds to intensive wave breaking and enhanced exchange processes caused by the presence of giant droplets. Inconsistency in C_d at high-wind speeds was also reported, with C_d saturating at approximately 25–35 m s^{-1} (Komori et al. 2018; Curcic and Haus 2020) rather than "rolling off" above 30 m s^{-1} (Jarosz et al. 2007; Kudryavtsev et al. 2019a; 2019b). Of note, Jarosz et al. (2007) and Kudryavtsev et al. (2019a, b) estimated C_d using the ocean response to TC winds and storm translation (i.e., a bottom-up approach).

Several reasons were offered in recent years to explain the inconsistency of C_d values at high-wind speeds. One explanation is that C_d is a function of Reynolds number and wave age rather than the often assumed 10-m wind speed (Donelan 2018). Similarly, the second explanation relates to a strong dependence of C_d on the sea state, based on both modeling (Chen et al. 2020) and observational studies (Zhou et al. 2022) of TCs. Zhou et al. (2022) reported that the most notable reduction of C_d occurs when the misalignment angle between the dominant wave direction and the wind direction exceeds about 45°, which is more common in the far front and in the left-front quadrant of the TC. This finding is consistent with the results from Holthuijsen et al. (2012). Additionally, the effects of shoaling waves on the variability of C_d at a given speed during TC landfall were reported by Chen et al. (2020), especially with steeper bottom slopes and faster moving TCs (Fig. 1). Chen et al. (2020) noted that C_d is particularly enhanced in the TC right-rear quadrant due to shoaling of fetch-limited waves and in the left-front quadrant due to shoaling of opposing-wind swells.

The third explanation for the inconsistency in the estimates of C_d relates to the applicability and accuracy of the flux-profile method of C_d estimation at hurricane-force wind speeds using dropsonde data from reconnaissance aircraft (Richter et al. 2021). Richter et al. (2021) specifically questioned the robustness of the decrease of C_d at 10-m wind speed >35 m s^{-1} and found large uncertainty in the estimation of C_d in high-wind conditions from consideration of the limited sample size alone (Fig. 2a). Other factors including the uncertainty in the height of recorded dropsonde data, the short vertical extent of the logarithmic layer, and violation of the assumptions of Monin-Obukhov similarity theory near the eyewall were also identified as potential contributors to a low-bias of C_d in high-wind conditions (i.e., the "rolloff" seen in earlier observational studies such as Jarosz et al. 2007). These results highlight the need for direct flux measurements in the lower hurricane boundary layer, such as through unmanned aircraft systems (Cione et al. 2020), to accurately estimate the C_d values at high winds.

b) Effects of C_d and Soil Moisture on TC Intensity Change

The role of C_d in TC intensification over the water was investigated in a recent idealized modeling study (Li and Wang 2021a). Li and Wang (2021a) found that a larger C_d induces stronger boundary layer inflow and shortens the spin-up period preceding rapid intensification (RI) than a smaller C_d. However, they found the intensification rate is unchanged if the

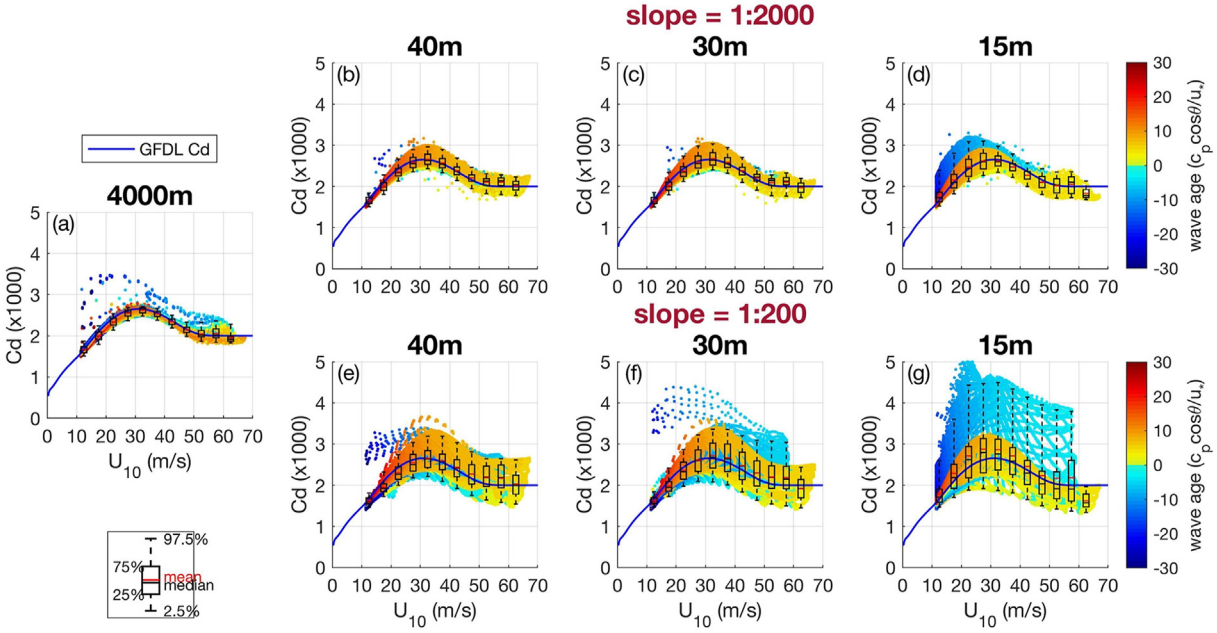

Fig. 1. C_d–U_{10} scatter plots in deep water (a) and at three different shallow-water depths, 40 m (b, e), 30 m (c, f), and 15 m (d, g), under a strong, fast-moving Category-5 TC. The upper panels (b–d) show results on 1:2000 (shallow) slope and the lower panels (e–g) show results on 1:200 (steep) slope. Data are color coded by wave age. The rectangular box with two whiskers shows data statistics in a given wind speed bin. The red and black lines in the box denote the mean and median C_d values, respectively. The bottom and top of the rectangular box mark the 25th and 75th percentiles of the C_d values. The lower and upper whisker levels indicate the 2.5th and 97.5th percentiles of the data. The blue line is the GFDL bulk C_d. From Fig. 11 of Chen et al. (2020).

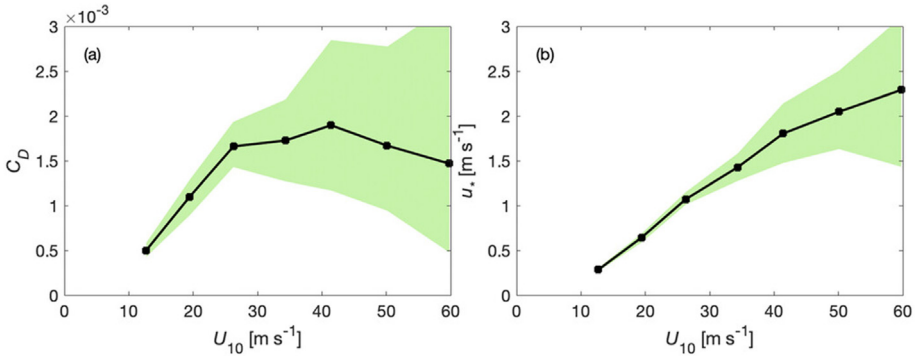

Fig. 2. The black squares show C_d calculated from all observational dropsondes over 1997–2018, and the shading represents the variability in C_d when performing 20 repeated tests of randomly subdividing the sonde database into thirds. (b) As in (a), but for friction velocity. From Fig. 6 in Richter et al. (2021).

variation of C_d is within a limited range, as effects due to frictional dissipation and C_d-modulated boundary layer inflow are nearly counteracted. Kim et al. (2022) further pointed out that reduced C_d in high winds also suppresses sea surface cooling; the extra energy drives TCs away from a steady state and they proposed that this explains the bimodality of the lifetime maximum intensity. Several recent studies (Chen and Chavas 2020; 2021; Hlywiak and Nolan 2021) also investigated the effects of C_d and soil moisture content on the intensity change of landfalling TCs, and agreed that surface roughening dominates over surface drying for the initial decay of wind speed after the landfall of TCs. This enhanced friction over land also enhances the overturning circulations. Hlywiak and Nolan (2021) also recognized the important role of higher soil moisture content in supporting more convection in the outer-core region that helps maintain or slows the decay of outer-core winds as the TC weakens and moves further inland, while the decay rate near the radius of maximum wind (RMW) is similar across different soil moisture contents.

c) Effects of Sea Surface Temperature and Surface Enthalpy Flux

Recent studies have advanced our understanding of the role of sea surface temperature (SST) and surface enthalpy flux (SFX) in TC intensification. In a real-case modeling study, Peng and Wu (2020) identified the key region where surface enthalpy flux is crucial to TC intensification. They found that a TC intensifies only marginally if the SFX is suppressed immediately outside the RMW, while a TC can intensify much faster if the SFX outside of a radius of about 2.5 times the RMW is suppressed, as deep convection aggregates inside the inner core and is suppressed in the outer core. In parallel, the impacts of anomalously warm SST in the pre-landfall RI of a supertyphoon were investigated by Chen et al. (2018a). They found that compared to relatively cool SST experiments, RI onset in the warmer SST experiments occurs much earlier due to earlier RMW contraction and more symmetric precipitation around the TC center, and the longer duration of the RI period before landfall in the warmer SST experiments leads to a much stronger TC at landfall. Interestingly, Kaplan et al. (2010) also found that TCs with a more symmetric inner-core structure as deduced based upon GOES-IR imagery were more likely to undergo RI. In a follow-up to their earlier study, Chen et al. (2021) further attributed the higher precipitation symmetrization before RI onset in the warmer SST experiments to a more effective boundary layer recovery of downdraft-cooled parcels that contributes to the development of upshear deep convection. A recent real-case observational study (Wadler et al. 2021) and dropsonde composite analysis (Nguyen et al. 2019) also highlighted the importance of left-of-shear high enthalpy fluxes in boundary layer recovery and the maintanence of upshear updrafts during RI. These studies emphasized that an accurate representation of surface fluxes is essential for the accurate prediction of TC intensity changes.

2.2. Boundary layer processes and eyewall turbulent mixing

A poor understanding and limited modeling of boundary-layer turbulent processes in numerical weather prediction (NWP) models are recognized as a key obstacle for TC intensity forecasts (e.g., Emanuel 2017). As existing planetary boundary layer (PBL) parameterizations in NWP models have generally been developed for non-TC conditions, researchers in the past four years collected additional measurements of turbulence properties and used large-eddy simulations (LES) to reveal the uncertainties of existing PBL schemes in TC conditions, both over the ocean and land, and to improve these schemes for better TC forecasts. Additionally, other topics including the role of eyewall turbulent mixing in modulating TC intensity change, PBL structure evolution during landfall, and the performance of PBL or canopy schemes over land are drawing increasing attention.

a) Boundary Layer Turbulence Observations

One of the greatest uncertainties of PBL schemes in hurricane conditions lies in the parameterizations of eddy viscosity, K_m, which relates downgradient vertical momentum flux to the local vertical wind shear (VWS). K_m is parameterized differently in various types of PBL schemes and is a function of turbulence kinetic energy (TKE) and mixing length in high-order PBL schemes. Retrieving K_m and related turbulence

properties in the TC PBL is of great value in evaluating PBL schemes in intense TC conditions. In recent years, additional measurements of turbulence properties were collected by different observational platforms, including multi-level towers sitting oversea or near the coast (Tang et al. 2018; Huang et al. 2022; He et al. 2022), lidar wind profilers (Tsai et al. 2019), manned aircraft (Sparks et al. 2019; Zhao et al. 2020), and small unmanned aircraft systems (sUAS, Cione et al. 2020).

During TC landfalls, Monin–Obukhov similarity theory was found applicable to the surface-layer horizontal and vertical wind speeds that exhibit logarithmic characteristics with height (Tsai et al. 2019; Huang et al. 2022), regardless of the nonstationary and spatially inhomogeneous conditions. The surface layer depth over land varies in different studies, from 60 m (Tang et al. 2018) to ~200 m (Tsai et al. 2019; He et al. 2022).

Over the ocean, the relationship between K_m and wind speed at flight level shows a lack of consistency among several studies. For example, an exponential increase of K_m with wind speed under high-wind conditions in the inner-core region from Sparks et al. (2019) differs from a nearly linear relationship between K_m and wind speed indicated by previous observations in North Atlantic hurricanes (e.g., Zhang et al. 2011). Zhao et al. (2020) instead identified a power-law increase of K_m with wind speed up to 40 m s^{-1} before leveling off. Additionally, Zhao et al. (2020) reported that the K_m values are ~50–100 m^2 s^2 in the eyewall within the 400–700 m layer, while in the same layer the mixing length does not vary much. One emerging technology to note is the sUAS, which is released from the National Oceanic and Atmospheric Administration (NOAA)'s P-3 reconnaissance aircraft to sample the turbulence properties within the lower hurricane boundary layer (Cione et al. 2020). The estimates of momentum stress from the sUAS were found encouragingly similar to previous measurements derived from NOAA P-3 manned aircraft and add to the understanding of turbulence characteristics in the inflow layer and eyewall.

b) Boundary-Layer Parameterizations and Modeling

The fact that PBL schemes are designed as single-column models motivates efforts to obtain K_m profiles in the TC PBL to assess PBL parameterizations. As the observed K_m profile over the ocean is only available at relatively weak wind speeds (18–30 m s^{-1}), Chen et al. (2021a) recently developed a modeling framework based on LES to obtain K_m profiles at hurricane-force wind speeds. This framework allows LESs to run under thermodynamic conditions from actual mature hurricanes; with this special setup, the LES produces reasonable values of effective K_m, momentum flux, and turbulence length scale compared to observations (Fig. 3). Evaluation of different types of PBL parameterizations using this framework and LES data reveals intrinsic deficiencies of *K*-profile parameterization (KPP) schemes in hurricane conditions, supports an asymptotic length scale of ~40 m for the Louis-type PBL parameterizations, and provides guidance to improve a high-order PBL scheme used in NOAA's next-generation hurricane forecast model Hurricane Analysis and Forecast System (HAFS) (Chen et al. 2021a; 2022). For KPP schemes, LES results indicate that the exponent in the parametric *K* profile needs to be increased for hurricane conditions such that the maximum K_m is located closer to the surface and reduced in magnitude. Two approaches to improve KPP schemes were subsequently proposed by Chen (2022). Analysis of the high-order Mellor–Yamada–Nakanishi–Niino (MYNN) scheme further supports a "three-layer" strategy for the mixing length

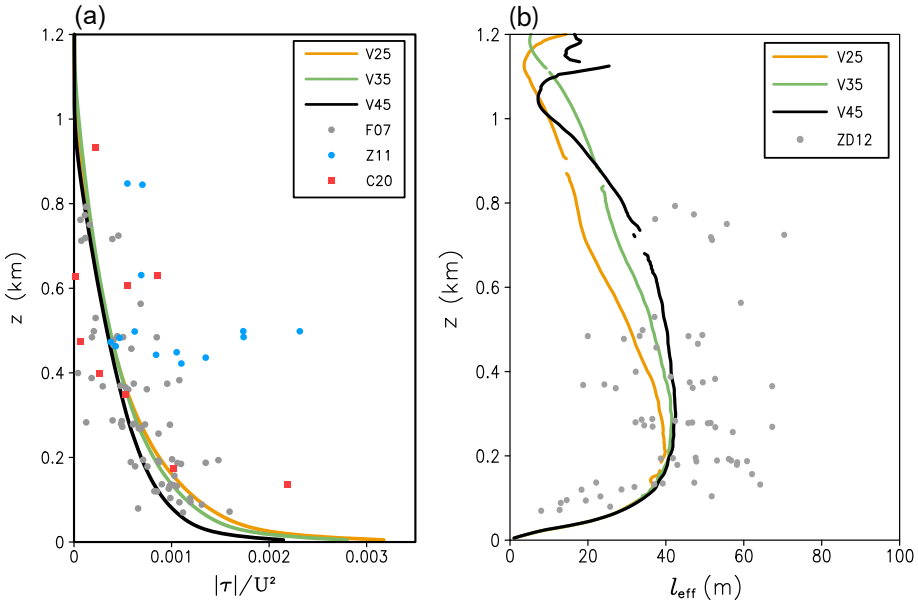

Fig. 3. Vertical profiles of nondimensionalized vertical turbulent momentum flux τ (m^2 s^{-2}) from three LES experiments where the surface wind speed is 25 m s^{-1} (V25, orange), 35 m s^{-1} (V35, green), and 45 m s^{-1} (V45, black). Gray and blue dots denote previous aircraft observations, and red dots denote the sUAS data from Cione et al. (2020). (b) Vertical profiles of the effective mixing length l_{eff} from the three LES experiments. Adapted from Figs. 7 and 11 in Chen et al. (2021a).

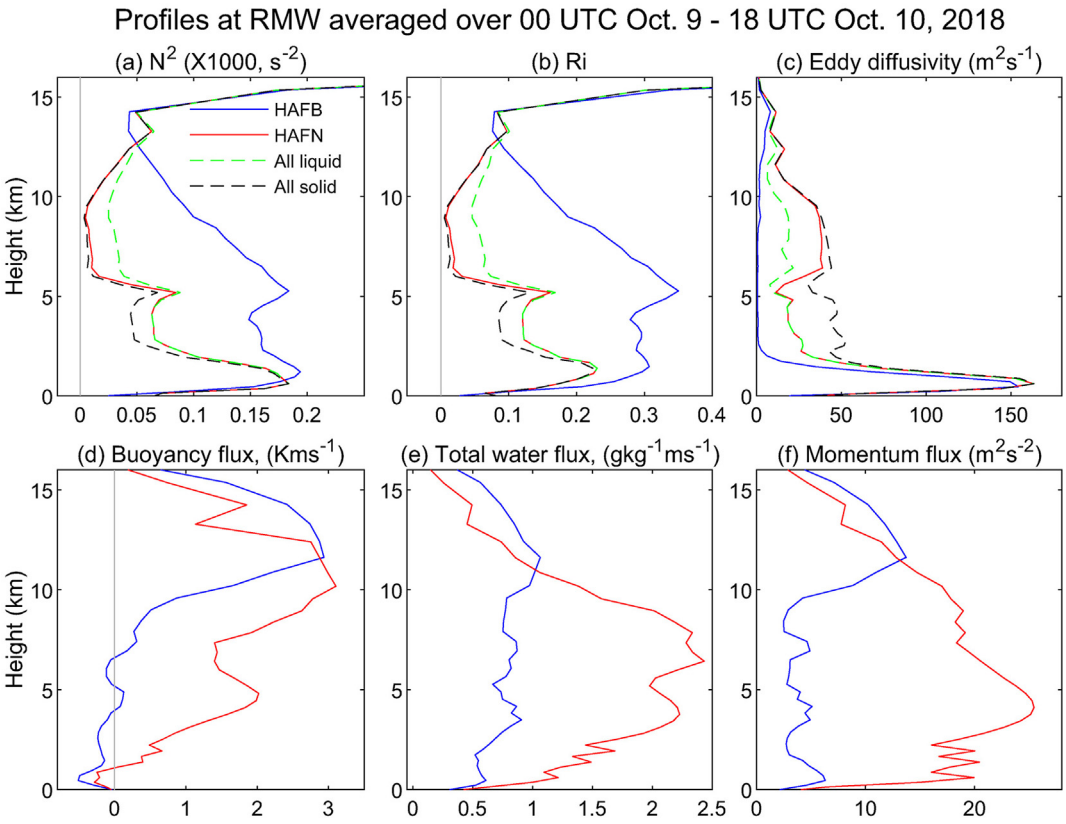

Fig. 4. Vertical profiles of azimuthal-mean N^2, Ri, K_m, buoyancy fluxes, total water fluxes, and momentum fluxes at the RMW averaged over the period from 0000 UTC 9 October to 1800 UTC 10 October 2018 simulated by HAFB (blue, original PBL) and HAFN (red, improved PBL). The fluxes shown in (d–f) include both model-resolved and sub-grid scale components. The green dashed and black dashed lines in (a–c) indicate the profiles of N^2, Ri, K_m calculated by treating cloud condensates as "all liquid" and "all ice," respectively. From Fig. 8 in Zhu et al. (2021).

parameterization for TCs that represents different types of turbulence regimes (Chen 2022). Another study that used LES to improve a PBL scheme is Li and Pu (2021), who included the effects of coherent large eddies into the K_m parameterizations within a KPP PBL scheme and further showed that the modified PBL scheme can improve intensity forecasts, though these interesting results are based on two available hurricane cases.

Additionally, efforts using flight-level observations to evaluate and improve PBL schemes were performed by Gopalakrishnan et al. (2021) and Hazelton et al. (2022). Other notable sources of uncertainty in the PBL schemes include the Prandtl number, which controls the ratios of momentum to moisture and heat exchange in the boundary layer (Kalina et al. 2021), and scale-aware parameterizations in the gray zone (Chen et al. 2021b), both of which have a strong impact in controlling the boundary layer structure and TC intensification. Of note, HAFS adopts a scale-aware PBL scheme, and efforts are desired to address the uncertainty in scale-aware parameterizations for future sub-kilometer numerical modeling.

c) Eyewall Turbulent Mixing

Vertical turbulent transport above the diagnosed PBL height, especially in the eyewall region, and its impact on TC intensity changes were recognized in recent studies. Zhu et al. (2021) identified an underprediction of in-cloud turbulent mixing above the PBL within a KPP PBL scheme and fixed this issue by including the effects of multi-phase water in the static stability calculation (Fig. 4a and b). The enhanced vertical turbulent mixing within the eyewall (Figs. 4c–f) contributes to stronger TC intensity and a smaller RMW based on the statistics of over 100 forecast cycles. Chen and Bryan (2021) investigated the role of TKE advection in idealized three-dimensional numerical simulations using a modified high-order MYNN scheme. They found that the vertical TKE advection is the predominant contributor to the formation of a deep TKE column in TC eyewalls, a structure that is comparable to the previous airborne Doppler radar observations, while the buoyancy TKE production in the eyewall remains negative above the near-surface layer due to the dominant stratification effect. Additionally, with the inclusion of TKE advection, especially vertical TKE advection, the simulated TC is stronger and the inner core is smaller, demonstrating that the TKE advection cannot be neglected in the TC modeling using a TKE-based PBL scheme.

d) Performance of PBL and Canopy Schemes During Landfall

The effects of PBL parameterizations on the surface wind field over land have been discussed in recent years. Nolan et al.

(2021a, b) carried out numerical simulations of Hurricane Wilma (2005) to understand the evolution of the boundary and surface layers over land. A key finding of their work was that if short-term TC forecasts can accurately predict the track, intensity, and size they can provide useful information on the timing and magnitude of peak winds at fixed points over land. Hendricks et al. (2021) extended that work to understand how well urban canopy models (UCMs) can predict winds in a major city during a TC's landfall. Near-surface winds in the urban area were strongly sensitive to the UCM and less sensitive to the boundary-layer parameterization. Although the UCM had a negative wind bias, it was able to produce realistic, heterogeneous wind patterns in the city.

e) Boundary-layer Structure (Including Landfall)

The boundary layer structure is closely related to TC intensity change. This important relationship has drawn the attention of researchers over the past four years. By examining the axisymmetric structure of the inner-core boundary layer for different intensity change groups using a dropsonde composite analysis, Ahern et al. (2019) found that compared to non-intensifying TCs, intensifying TCs have a deeper tangential wind jet and, thus, higher inertial stability in the eyewall region and lower static stability above the near-surface inflow outside the eyewall. These differences in the PBL structure indicate a higher possibility of low-level ascent outside of the RMW in non-intensifying TCs. In a modeling study of a TC, Ahern et al. (2021) revealed that the formation of descending inflow in response to increased shear during the weakening stage provides an ideal downward conduit for low-entropy parcels into the inner-core boundary layer. This hampers convective development azimuthally downwind of the inflow. Dynamically, the descending inflow accelerates the tangential wind in the downshear-left quadrant and immediately downwind, while the primary circulation in the right-of-shear quadrant weakens with time.

A distinctive kinematic feature in the TC PBL is the supergradient wind. Recent idealized simulation studies agree on the minor contribution of vertical advection of supergradient wind to the intensification rate while they diverge on its contribution to the steady-state intensity, ranging from 10–15% in axisymmetric simulations (Li et al. 2020) to more marginal fractions in 3D simulations (Fei et al. 2021).

Strong VWS and nearly-neutral stratification in TC PBLs provide ideal conditions for the formation of roll vortices. Studies in recent years documented different types of rolls or coherent structures in the TC PBLs (Gao and Ginis 2018; Guimond et al. 2018; Sroka and Guimond 2021; Tang et al. 2021). Tang et al. (2021) confirmed the existence of roll vortices with wavelengths of 400–1600 m in the outer-core region in two typhoons and further quantified that the averaged momentum flux of flight legs with rolls was ~2.5 times that of legs without rolls at a similar wind speed range. The characteristics of linear-phase rolls under a moving hurricane were investigated by Gao and Ginis (2018), who found that the horizontal wavelength of rolls is determined by the radial-shear-layer depth. A key finding in Gao and Ginis (2018) is that the roll growth rate is not only determined by radial wind shear magnitude but also by the radial-shear-layer depth. Rolls under a deeper shear layer have large size and thus are more easily affected by the bottom boundary, which reduces the efficiency of rolls in extracting kinetic energy from the mean flow.

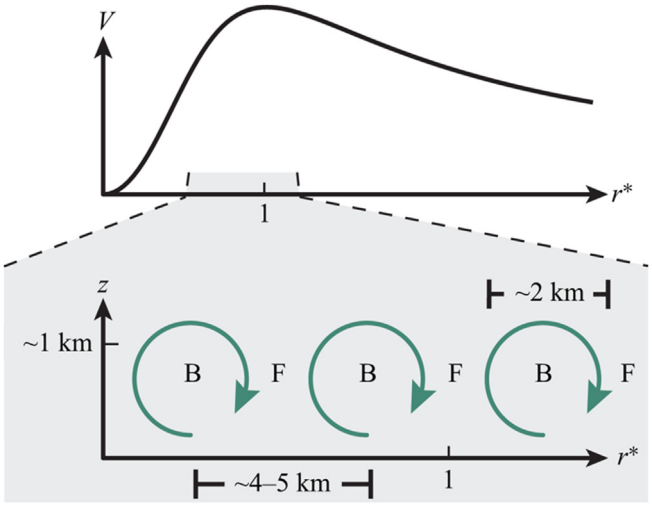

Fig. 5. The upper panel shows a typical azimuthal mean wind profile in a mature hurricane where the radial coordinate is normalized by the radius of maximum wind. The lower panel shows a conceptual diagram of the observed secondary circulations associated with boundary layer eddies and the phasing of peaks in forward scatter (F) and backscatter (B). From Fig. 20 in Sroka and Guimond (2021).

In contrast, Guimond et al. (2018) identified a different type of coherent turbulent eddy during an eyewall replacement cycle of Hurricane Rita (2005). These coherent eddies have a radial wavelength of ~1–3 km and depth of ~1.5 km and, more importantly, these eddies transport high-momentum air upward, in contrast with roll vortices (Fig. 5). Sroka and Guimond (2021) further quantified the effects of upscale energy transfer (or backscatter) of these coherent eddies on TC vortex intensity by computing the kinetic energy budget for the resolved-scale and eddy-scale motions. While the sub-filter-scale (<2 km) energy transfer term was found to be a minor contributor to the resolved-scale kinetic energy, it contributes an average of ~30% to the local time tendency of eddy-scale kinetic energy. This result indicates that the primary dynamical pathway for the coherent turbulent eddies to influence the TC vortex is through wave–wave nonlinear interactions, which can subsequently influence the wave–mean flow interactions. These different types of coherent structures in the TC PBL call for more future endeavors to investigate their formation mechanisms.

The wind and storm surge damage of landfalling hurricanes emphasize the need to understand the evolution of boundary layer structure during and post-landfall. A Doppler-radar analysis of Hurricane Irene (2011) by Alford et al. (2020) documented a transition of the tangential wind jet from within the boundary layer over water to above the boundary layer onshore; this transition occurred within the distance of

5 km inland. The lofted tangential wind jet during coastal transition is an outcome of reduced maximum tangential wind within the TC PBL, a response to greater surface roughness on shore, and nearly-intact tangential wind above. Hlywiak and Nolan (2022) examined the modification of boundary layer wind fields of idealized powerful TCs forced by the coastal roughness discontinuity before landfall. They found the sudden decrease in frictional stress of highly agradient flow crossing the offshore coastline contributes to enhanced off-shore radial and vertical velocities once the TC is within roughly 200 km of land. The enhanced advection of angular momentum by the secondary circulation downstream accounts for the enhanced upper boundary layer winds to the rear and rear-right relative to TC motion, which may lead to stronger, more damaging downdraft-related gusts in that region of the storm.

2.3. Microphysics and precipitation processes

Several recent studies have examined the relationship between the spatial distributions of precipitation, associated latent heating profiles, and the TC vortex response to such heating distributions. Much of this work has focused on weak TCs, including those prior to genesis as well as tropical depressions and tropical storms, to describe how precipitation processes help to organize these weak systems to a point where intensification can occur. Bell and Montgomery (2019) used aircraft data to investigate the mesoscale processes leading to the genesis of Hurricane Karl (2010). They found that the convective cycle in Karl, diurnally alternating between convective precipitation that stretched vorticity in the lower troposphere and stratiform rainfall that amplified the mid-level vorticity, spun up the vortex in low levels and led to Karl's genesis. The onset of deep convection and associated low-level spinup were closely related to the coupling of the vorticity and moisture fields at low- and mid-levels, and this study reaffirmed the primary role of deep convection in the genesis process while providing a hypothesis for the supporting role of stratiform precipitation and the mid-level vortex. Nam and Bell (2021) emphasized the role of tilting of vorticity in cumulus congestus clouds and subsequent stretching of vorticity in the lower troposphere from deep convection to explain how a low-level vortex could persist in the presence of substantial VWS until genesis occurred.

Rogers et al. (2020) extended these ideas from genesis to downshear reformation, when they examined the role of precipitation processes in the reformation and subsequent intensification of the weak TC that became Hurricane Hermine (2016). They noted that while Hermine was initially tilted under moderate VWS, repeated cycles of deep convection on the downshear side contributed to the formation of a downshear environment characterized by a low instability index and high column moisture, a condition known to favor bottom-heavy mass flux profiles and low-level vorticity stretching (Raymond et al. 2014; Sessions et al. 2015; Sentic et al. 2015; Raymond and Flores 2016; Raymond and Kilroy 2019; Raymond and Fuchs 2021). Under these thermodynamic conditions, a subsequent burst of deep convection successfully repositioned the low-level center underneath the well-developed mid-level center (or reformation) and affected the subsequent intensification. Alvey et al. (2022) showed a similar alignment process in Hurricane Dorian (2019), using ground-based and airborne radar to show that deep and moderate convection, at least partly driven by terrain interactions with the island of Martinique, led to a repositioning of the low-level vortex closer to the mid-level vortex and in a more humid environment (e.g., Fig. 6). Further removed from ventilation and in a more nearly-aligned state, Dorian commenced RI.

While the studies mentioned above focused on the vertical structure of latent heating and mass flux profiles, other recent work has examined the azimuthal variation of precipitation and its impact on TC intensity change. Chen et al. (2018a), in a set of simulations of the RI of Typhoon Mujigae (2015), found that precipitation became more symmetrically distributed around the vortex as vortex tilt decreased. In the simulation where RI onset occurred earlier, precipitation symmetry was higher in the inner-core region, particularly for stratiform precipitation. The presence of the aligned vortex, precipitation symmetry, and strong boundary layer inflow at the RMW led to a contraction of the RMW and the formation of a strong and compact inner core, which was the key component explaining RI onset.

Intensity forecasts are sensitive to the representation of microphysical processes in numerical models (Park et al. 2020; Wu and Coauthors, 2021), and several recent studies have improved our understanding of these processes. Feng and Bell (2018) used polarimetric radar observations to show that the precipitation asymmetry in major Hurricane Harvey (2017) was due to an asymmetric updraft induced by vertical shear, hydrometeor size sorting, and a convective to stratiform transition in the rotating flow. Microphysical asymmetries and the size sorting signature are prevalent in intense hurricanes (Homeyer and Coauthors, 2021) and may also be induced by storm motion (Didlake and Kumjian 2018) or vortex Rossby waves (Huang et al. 2022). Variations in microphysics also occur radially, with warm-rain processes generally dominant in the inner rainbands with an increasing importance of ice-phase processes and graupel production in outer rainbands (Wu et al. 2018; DeHart and Bell 2020). These microphysical variations in both azimuth and radius have dynamic impacts through modification of the distribution of latent heating and evaporative cooling, which can lead to intensity change and eyewall replacement cycles (ERCs). The importance of stratiform precipitation processes in the ERC process in particular has been emphasized in recent studies (see Section 2.5c).

The ability of deep convection to ventilate the air from the top of the boundary layer was recognized to be an important process regulating TC intensity change (e.g., rapid decay) in a recent idealized modeling study. Smith et al. (2021) found that the rapid decay of the TC vortex results from the increasing difficulty of deep convection to ventilate the air exiting the boundary layer, resulting in unventilated air being advected radially outwards in the lower troposphere and leading to spin-down because of the approximate conservation of mean absolute angular momentum. Smith et al. (2021) also pointed out

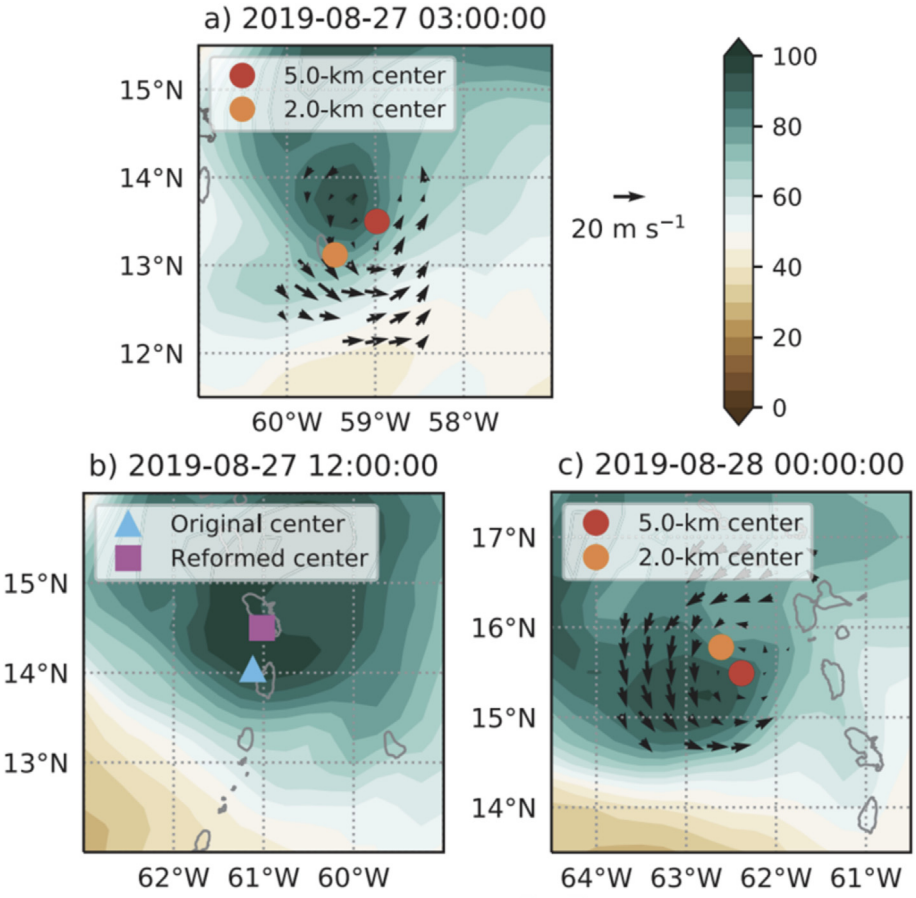

Fig. 6. An example of downshear reformation as seen in 700–500-hPa layer-mean relative humidity (RH; shaded; %) from the ECMWF Reanalysis Version 5 (ERA5) data at three successive times over a 21-h period. Storm-relative winds at a height of 5 km (black vectors), along with 2- and 5-km TC center estimates, are shown when tail-Doppler radar observations from a NOAA WP3 mission were available (a and c). Figure adapted from Fig. 6 in Alvey et al. (2022).

the possibility of misinterpreting this pathway as an outcome of ambient VWS, if rapid decay was found in real TCs under VWS.

2.4. Radiative feedbacks

Over the last four years, observational and numerical modeling studies have continued to investigate the diurnal variation in TC structure, which usually manifests as radially-outward propagating pulses of anomalously cold infrared (IR) brightness temperatures over a deep layer of the troposphere (Dunion et al. 2019). Moderate or strong diurnal signals can be observed in 45%, 54%, and 61% of at least tropical storm-, hurricane-, and major hurricane-strength TC cases (Knaff et al. 2019). Similar percentages were found by Ditcheck et al. (2019a). That 36-y climatology of Atlantic basin TC diurnal pulses not only identified cooling pulses, but also uncovered pulses of warmer IR brightness temperatures propagating outward following the Dunion "diurnal clock" (Dunion et al. 2014; Ditchek et al. 2019a). Ditchek et al. (2019b) further grouped pulses into electrically-active (ACT), quasi-electrically active (QUASI), and inactive pulses (INACT) based on World Wide Lightning Location Network (WWLLN) lightning activity. The propagation of ACT cooling pulses, ACT warming pulses, and INACT cooling pulses lent support to the gravity wave interpretation of diurnal pulses (Ruppert and O'Neill 2019; Evans and Nolan 2019) and to the tropical squall-line characteristics after propagating away from the inner core (Dunion et al. 2019; Ditchek et al. 2020).

In addition to diurnal IR brightness temperature variations, the transverse circulation of TCs in numerical simulations has a bimodal diurnal evolution with peaks from low-to mid-levels nocturnally and in the upper troposphere during daytime (Ruppert and O'Neill 2019; Evans and Nolan 2022). Observations using composite analyses of GPS dropsondes (Zhang et al. 2020) and satellite sounding retrievals (Duran et al. 2021) reveal the diurnal variation of the mean PBL structure with much stronger inflow during nighttime, leading to the contraction of the RMW (Tang et al. 2019; Wu and Hong 2022) and the size of eye (Lee et al. 2020), which, in turn, leads to an increase in the intensity of the TC (Wu et al. 2020). Finally, rapidly intensifying TCs have been found to have a greater diurnal variation of overshooting tops (Sun et al. 2021), a higher frequency of long-duration pulses, and a significantly longer mean pulse duration than steady-state and gradually intensifying TCs (Zhang and Xu, 2021).

Besides the diurnal variation in TC structure, efforts have also been put forward to understand the impact of

cloud–radiation feedback on TC genesis and intensification, inspired by its critical role in convective aggregation. Recent studies using the idealized framework of rotating radiative–convective equilibrium suggest that the radiative feedbacks are sufficient to form organized convective clusters and, thus, a weak cyclone, and can significantly accelerate cyclogenesis by a factor of two or three (Muller and Romps 2018; Carsten and Wing 2022; Wing 2022). The acceleration of TC genesis occurs due to horizontally and vertically varying radiative feedbacks that favor the development of the mid-level vortex (Carstens et al. 2020; Yang and Tan 2020; Wing 2022). The overall impact of radiative feedback on TC genesis is also a function of vortex strength. All else being equal, a stronger initial vortex reduces the impact that radiation has on accelerating tropical cyclogenesis (Smith et al. 2020). After genesis, cloud-radiation feedbacks can prevent tropical cyclones from reaching a higher intensity by establishing a more tilted eyewall that is unfavorable for stronger inward transport of absolute vertical vorticity (Yang et al. 2022). Cloud–radiation feedback can also affect the timing and variability of structure changes of TCs (Trabing et al. 2021) under different background environments, such as large-scale VWS (Rios-Berrios 2020) and tropopause temperature (Trabing et al. 2019).

The relevance of such idealized simulations to real-world TCs, which form from pre-existing disturbances, remains unclear. Focused on Super Typhoon Haiyan (2013) and Hurricane Maria (2017), Ruppert et al. (2020) demonstrate that the cloud–infrared radiation feedback, referred to as the "cloud greenhouse effect", provides moist static energy to the incipient storm and directly promotes the thermally-direct transverse circulation that moistens the storm core and, in turn, favors TC intensification via the wind-induced surface heat exchange (WISHE) feedback. The formation of Typhoon Haiyan was also accelerated through the cloud–radiation feedback by enhancing the mid-level circulation via potential vorticity production (Yang et al., 2021a). Climate simulations with realistic boundary conditions suggest that radiative feedbacks do contribute to TC development (Wing et al. 2019) and suppressing radiative interactions can reduce the global TC frequency due to a decrease in the frequency of pre-TC synoptic disturbances (Zhang et al. 2021). Besides numerical simulations, observations also provide evidence on the favorable role of radiation in TC development. Wu et al. (2021) found that intensifying TCs have greater radiative heating from clouds within the TC than weakening ones. TCs with enhanced cloud radiative effects tend to intensify, especially for those with weak initial intensity.

2.5. TC structure

a) Vortex Shape

The impact of TC horizontal structure on TC intensity has received a lot of attention while the influence of TC vertical structure on intensity is a new emerging topic. Progress in both areas is summarized below.

Absolute angular momentum is intrinsically tied to vortex structure and it is integral to the dynamical evolution of TC structure and intensity. For instance, Peng et al. (2018, 2019) investigated relationships between angular momentum and intensity change. In their studies, the intensification stage is divided into Phase I and Phase II according to the state of slantwise moist neutrality. During Phase I, the intensification is accompanied by the conversion in the angle between absolute angular momentum surfaces (M) and entropy surfaces (s) from almost orthogonal to congruent inside the inner core (Peng et al. 2019). During this process, the sporadic, deep convection near the RMW plays an important role in vertically redistributing the large M and s from the lower troposphere upward to the tropopause. Later, Peng and Fang (2021) explored how the vertical depth of the initial vortex impacts the early evolution of simulated TCs in Phase I. They found that a shallower vortex has a stable low-level stratification which inhibits deep convective bursts and results in slow development of slantwise moist neutrality. The longer time it takes in Phase I, the slower the TC intensifies during the early stage. A state of slantwise moist neutrality is gradually approached during Phase I, which leads to Phase II, when the intensification theory of Emanuel (2012) applies with the congruency between M and s surfaces (Peng et al. 2018). Hence, the timing of Phase I partially determines the timing of TC intensification.

A recent observational study on Hurricane Michael (2018) (DesRosiers et al. 2022) also showed that TC RI is accompanied by the redistribution of the M surfaces in the inner core region. Three-dimensional kinematic fields of the storm, which were retrieved from tail Doppler radar data, exhibited a steepening of the inner core M surfaces (Fig. 7) during Hurricane Michael's RI stage. This progression is attributed to the eyewall updraft.

In the above-mentioned studies, TC intensification is shown to depend on and co-evolve with the vertical structure of the parent vortex. These findings emphasize the importance of carefully considering the details of vertical structure in addition to the horizontal structure in TC initialization and forecast validations.

Another valuable area of vortex structure research has further emphasized the importance of the outer TC structure on intensity. Guo and Tan (2022) used the concept of TC fullness (Guo and Tan 2017) to shed new light on TC intensification rate. Fullness represents the ratio of the extent of the outer-core wind skirt (i.e., the region between the RMW and gale-force wind radius) to the outer-core size of the TC, and it accounts for the observation that TC size (defined by a single size metric such as RMW or gale-force wind radius) and intensity are not necessarily correlated. The fullness increases as the outer-core size increases and/or the inner-core size decreases. Guo and Tan (2022) showed that large values of TC fullness are associated with high intensification rates.

Li and Wang (2021b) proposed that the sensitivity of the TC intensification rate to the inner-core size and the outer-core wind structure results primarily from the fact that surface enthalpy fluxes outside the RMW contribute to the eyewall

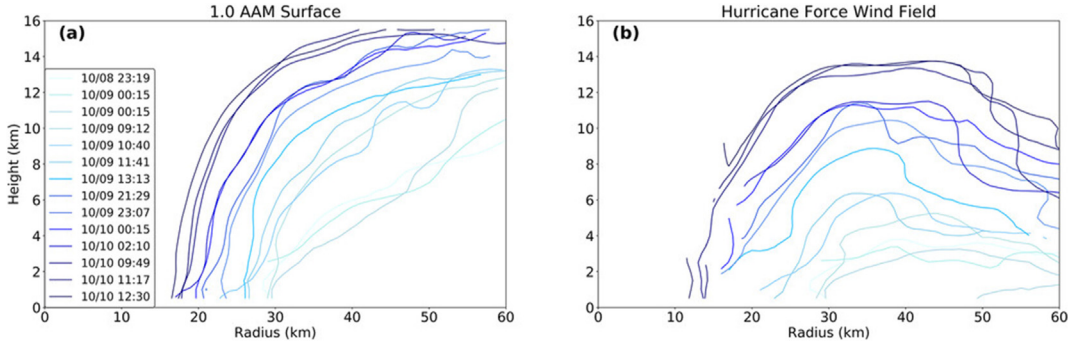

Fig. 7. (a) Progression of the azimuthally-averaged 10^6 m^2 s^{-1} absolute angular momentum (AAM) contour, and (b) hurricane-force wind contour (33 m s^{-1}) during 14 aircraft passes in Hurricane Michael (2018). Adapted from Fig. 3 in DesRosiers et al. (2022).

entropy budget and diabatic heating while the surface stress is largely determined by the surface wind near the RMW (namely the TC intensity) only. More recently, sensitivity of the initial TC spinup and subsequent intensification rate to the initial wind profile inside the RMW was reported by Li et al. (2022b), who showed that higher winds inside the RMW favor a shorter initial spinup period and higher intensification rate, especially for TC vortices with a relatively large RMW. On one hand, higher winds inside the RMW promote stronger surface enthalpy fluxes that support faster inner-core moistening and convective organization (or faster initial spinup). On the other hand, stronger winds inside the RMW imply higher inertial stability that contributes to higher efficiency of eyewall diabatic heating and higher intensification rates.

The above findings suggest that a realistic representation of the initial TC structure is key to skillful TC intensity forecasts by numerical models, and highlight the need for routine observations of the inner-core kinematic structure of TCs.

b) Vortex Alignment

TC intensification, and RI in particular, typically begins when TCs are weak. For example, Wang and Jiang (2021) showed that ~75% of all RI events initially had intensities of 55 kt or less, which is similar to the results of an earlier study by Kaplan et al. (2010) that indicated ~60–70% of RI events in the Atlantic and Eastern Pacific basins, respectively, occurred for TCs whose initially intensity was 60 kt or less. Structurally, the development of a vertically-aligned circulation is a key step to drive RI onset (e.g., Chen et al. 2019; Tao and Zhang 2019; Alvey et al. 2020; Schecter 2022) or prevent TCs from continuous decaying (Liu et al. 2021), as an aligned circulation promotes a symmetric distribution of precipitation and increases resilience to the ventilation induced by VWS (Chen et al., 2018a, 2019; Ryglicki et al. 2019; Alland et al. 2021a, 2021b; Fischer et al. 2022). Understanding how alignment occurs, however, is particularly challenging for weak TCs, since they have a weak rotational constraint and are, hence, dominated by divergent flow, rendering them more vulnerable to hostile environments (e.g., dry air, VWS) than stronger TCs. Identifying structural characteristics associated with aligning, rapidly-intensifying weak TCs is therefore an important step in understanding the physical processes underlying RI onset.

Recent studies involving idealized modeling, real-case simulations, and observational case study analyses have identified two alignment pathways. Both pathways involve the mutual advection of the low-level vortex and mid-level vortex toward one another, with a key distinction between the pathways being their respective emphasis on divergent vs. non-divergent flow in facilitating alignment (both pathways could of course occur simultaneously in nature).

The first (non-divergent) pathway is the precession of the mid-level vortex into the upshear quadrants, where it can then be advected near the low-level vortex by the background environmental VWS (Rios-Berrios et al. 2018; Gu et al. 2019). The precession of the mid-level vortex can be sensitive to how the background wind veers with height, as cyclonic (anticyclonic) rotating shear accelerates (decelerates) the precession rate through the feedback between moist convection and the balanced response to the height-dependent vortex tilt (Gu et al. 2018; 2019). The second (divergent) pathway includes the advection of the low-level vortex toward the location of the mid-level vortex, which can be facilitated by convectively-driven inflow toward regions of deep convection co-located with the mid-level vortex (e.g., Schecter and Menelaou 2020; Schecter 2022), and the local modulation of vorticity through diabatic processes. Modulation of vorticity by diabatic processes can take the form of either: 1) the reformation of a new smaller vorticity core or low-level circulation (LLC) either beneath or near the mid-level circulation (MLC) via persistent convection with a bottom-heavy vertical mass flux profile that facilitates lower-tropospheric vortex stretching (e.g., Chen et al. 2018b; Rogers et al. 2020; Alvey et al. 2022 – see accompanying discussion in subsection 2.3); 2) the vertical development of a low-level vortex upward, effectively generating a vertically aligned circulation (e.g., Miyamoto and Nolan 2018); or, 3) a "reconstructing" process in which vortex merger occurs to yield a single closed circulation over a deep layer (Rios-Berrios et al. 2018).

c) Rainbands

While it remains an open question whether rainband activity is favorable or unfavorable for TC intensity and intensification

(e.g., Wadler et al. 2022), most of the research over the last four years has elucidated the negative impacts of rainbands on intensity. Alland et al. (2021a, b) found that downdraft and radial ventilation [the downward and inward, respectively, transport of low equivalent potential (θ_e) air] occurs within, and downstream of, convection associated with rainbands, consistent with Riemer et al. (2010). Furthermore, the vertical structure of the ventilation suggests that weaker TCs embedded in environments that are drier and have larger VWS (thus larger vertical tilts) are associated with stronger ventilation extending lower down toward the surface, inhibiting convection and leading to less intensification. Hu and Wu (2020) also demonstrated the negative impact of rainbands on intensification using ensemble sensitivity analysis. They showed that when outer rainbands are active, mid-level inflow becomes stronger. Consequently, more low-θ_e air impinges into the boundary layer, decreasing θ_e radially inward towards the eyewall, and limiting TC intensification. In addition to ventilation, rainbands can also impede inflow from reaching the inner core, as demonstrated by Dai et al. (2019) who found that low-level inflow near the eyewall is enhanced in idealization simulations where an outer rainband is "damped" (through reduction of the water mixing ratio).

TC rainbands also play an important role in the formation of secondary eyewalls, which modulate TC intensity. Using Doppler radar observations collected in Hurricane Earl (2010), Didlake et al. (2018) documented mesoscale, mid-level, descending, radial inflow in the stratiform portion of a rainband, consistent with previous studies (e.g., Moon and Nolan 2010; Didlake and Houze 2013). As this descending inflow penetrated the inner core, enhanced convergence induced an intense updraft that appeared just prior to the occurrence of secondary eyewall formation. Recent idealized (Yu and Didlake 2019) and real-case (Zhu et al. 2022; Yu et al., 2021) simulations confirmed the results of Didlake et al. (2018) that the low-level updrafts generated on the inner edge of the stratiform portion of the rainband are capable of triggering convectively-buoyant updrafts that may further impact the intensity and structure evolution of the TC. Wang and Tan (2020) emphasized the essential role of unbalanced dynamics in the outer rainbands in the formation of a secondary eyewall. They found that the canonical formation of secondary eyewall results from the coupling between two different pathways, the wind-maximum formation pathway and the convective-ring pathway. Idealized TC simulations performed by Wang et al. (2019) show that the upper-tropospheric stratiform cloud in the outer rainband spirals cyclonically inward and downward and is axisymmetrized when the inner sector reaches the outer edge of the rapid filamentation zone in the boundary layer. Continuous axisymmetrization of the downwind inner sector in the boundary layer leads to the formation of a secondary eyewall. Environmental conditions (e.g., nonzero vertical wind shear) that favor the activity of outer rainbands can bridge the external and internal dynamics of secondary eyewall formation (Wang and Tan 2022). A five-year study of observed secondary eyewall formation (Vaughn et al. 2020) further highlights the potential importance of a stationary banding complex observed 12-h prior to secondary eyewall formation in 79% of their cases.

d) Eyewall Replacement Cycles

The internal TC phenomena of secondary eyewall formation (SEF) and eyewall replacement cycles (ERCs) significantly influence TC intensity. Typically, an ERC marks either a temporary or permanent break in TC intensification, particularly at a stage of evolution where concentric eyewalls are apparent to an observer. Currently, the variability in the ERC timescale presents the largest intensity prediction barrier. Recent studies shed light into this variability. Yang et al., (2021b) showed longer-lived ERCs are associated with larger outer eyewalls and typically transpire under relatively high sea-surface temperatures and weak VWS. Large moats appear favorable for increased boundary layer pumping in the inner eyewall and, therefore, a more intense inner eyewall (Kuo et al. 2022). More generally, intricacies in vortex structure and the environment likely play a role in ERC timing (e.g., Fischer et al. 2020). Overall, these results indicate that the variability in ERC timescale, and therefore the timing of intensity changes, is partly influenced by the size and configuration of concentric eyewalls and overall vortex structure. It is also important to note that TC-ocean feedbacks may further alter the ERC timescale from the climatological mean. For example, slower moving storms can induce enhanced sea surface cooling that accelerates the ERC process via rapid decay of the inner eyewall (Li et al., 2022a). In contrast, Yang et al. (2019) show ocean feedbacks can act in a diametrically opposed manner to the study of Li et al. (2022a) because ocean cooling may introduce energy flux asymmetries that slow the ERC. In either case, it is plausible that enhanced ocean feedbacks inhibit reintensification otherwise expected at the conclusion of an ERC. Finally, the presence of moderate VWS can alter the nature and timescale of ERCs (Dougherty et al. 2018; Wang and Tan 2022). The variance seen in ERC timescales guarantees continued predictive challenges arising because of ERCs.

e) Eyewall Instabilities

Eyewall barotropic instabilities related to strong horizontal shear reversals in the vicinity of the RMW manifest in different intensity change outcomes depending on the sophistication of the model, with two-dimensional barotropic models indicating wind speed decreases and pressure falls (Vigh et al. 2018) associated with mixing. On the other hand, sophisticated full-physics hurricane simulations often show further intensification in the presence of instabilities. The more realistic hurricane simulations, in fact, offer a wider spectrum of intensity outcomes dependent on the numerous multiscale factors at play, betraying simple rules of thumb for the forecaster.

Consistent with early 2D studies on eyewall barotropic instability, Mashiko and Shimada (2021) documented the observed evolution of polygonal eyewalls and mesovortices using Doppler radar and surface stations. They found that mesovortices possess pressure deficits and enhanced surface

winds. They also documented observational evidence of mixing of high equivalent potential air between the eye and eyewall. In terms of full-physics model results that show eyewall instabilities during intensification, recent detailed observational analyses demonstrate vividly the existence of polygonal eyewalls during periods of RI (Cha et al. 2020). There has also been a continuation of numerical investigations of the role of eyewall potential vorticity (PV) mixing in RI. Tsujino and Kuo (2020) used a full-physics simulation of Supertyphoon Haiyan (2013) in tandem with PV inversion and balanced dynamics diagnostics of model output to propound that PV mixing leads to pressure falls, enhanced boundary layer inflow at low levels, and intensification. On top of the significant progress made in observations and full-physics models, eyewall instabilities have been revisited in simplified barotropic models as well, including in the work of Jiang and Wang (2022) that shows barotropic instabilities in idealized vorticity rings advance more quickly and asymmetrically on a beta-plane than on an *f*-plane.

Eyewall instabilities are present in the scenario of concentric eyewalls too. In a series of papers, Lai et al. (2019, 2021a, b, c) used both simple, idealized models and full-physics models to examine the role of barotropic instability across the moat in the evolution of double-eyewall tropical cyclones. They showed that the associated eddy radial transport of absolute angular momentum resulting from the instability can make a substantial contribution to inner eyewall decay. This dynamical inner eyewall decay mechanism may be important in real TC eyewall replacement cycles, working simultaneously with other processes such as the boundary layer cutoff effect.

f) Relative time between eyewall contraction and rapid intensification

The contraction of a TC's RMW often accompanies intensification. However, recent observational and numerical studies (Stern et al. 2015; Qin et al. 2016; Li et al. 2019) indicate RMW contraction often stops well before the end of intensification. In fact, the observational study of Wu and Ruan (2021) shows rapid RMW contraction often precedes RI in North Atlantic TCs, with smaller RMWs being more efficient to intensify for a given heating rate. The idealized simulations of Li et al. (2021) provide insight into this sequence of events. They found that during the rapid RMW contraction stage, because of the weak TC intensity and large RMW, the negative moderate radial gradient of radial vorticity flux and small curvature of the radial tangential wind distribution across the RMW favor rapid RMW contraction. On the other hand, relatively small diabatic heating far inside the RMW leads to weak low-level inflow and small inward absolute vorticity flux near the RMW and thus a small intensification rate (Fig. 8a and 8c). Subsequently, the RMW contraction rate decreases quickly due to the rapid increase in the curvature of the radial tangential wind distribution across the RMW as the TC intensifies rapidly and the RMW decreases (Fig. 8b and 8d). Observational studies from Li et al. (2022c, 2022d) provide a detailed overview of the timing, relationships, and variability of TC RMW contraction and intensification. With such observed relationships well analyzed over many TCs, these studies may provide new practical guidance for predicting intensity changes including RI.

3. Intensity change theory and predictability

3.1. Time-dependent theories of TC intensification

In recent years, there has been a significant improvement in understanding the factors influencing TC intensification. Kieu et al. (2020) proposed a reduced dynamical model to study TC intensification. Based on the non-dimensional equations, they showed that with constant convective heating and frictional convergence in the absence of slantwise moist neutrality or surface fluxes (convective instability of the second kind mechanism, CISK) is able to generate intensification and a final stable maximum intensity, but the efficiency of this process decreases rapidly as the TC inner core approaches a state of moist neutrality, during which the WISHE feedback is responsible for TC intensification. This explains why CISK cannot support the intensification of real TCs. They also emphasized that TC intensification ultimately depends on the frictional convergence of absolute angular momentum inside the boundary layer no matter feedback mechanisms.

Quantitatively understanding TC intensification rate has long been a problem. Emanuel (2012) is the first study that attempted to develop a time-dependent theory of TC intensification based on the boundary layer momentum and entropy budget equations, and the assumptions of an axisymmetric vortex in thermal wind balance and slantwise moist neutrality in the eyewall ascent above the boundary layer. Using the constraint from the critical Richardson number in the outflow region, an extra relationship between dynamic and thermodynamic parameters (absolute angular momentum M and saturation entropy s^*) closes the governing equations and leads to a simple equation for intensification rate (Emanuel 2012):

$$\frac{\partial V_m}{\partial \tau} \approx \frac{C_k}{2h}\left(V_{max}^2 - V_m^2\right), \tag{1}$$

in which, V_m is the current maximum intensity, $V_{\max}$ is the steady-state maximum wind, and h is the boundary layer height.

However, as shown in an observational study by Xu and Wang (2018), the maximum potential intensification rate lies in the middle of the intensification stage, which is not consistent with the predicted intensification rate from Equation (1). Since then, several improved versions of Equation (1) have been proposed by Wang et al. (2021a, b, 2022).

In Wang et al. (2021a), a dynamical efficiency (E) is introduced in the intensification equation, such that

$$\frac{\partial V_m}{\partial t} \approx \frac{C_d}{H}\left(EV_{mpi}^2 - V_m^2\right), \tag{2}$$

where $E = \left(\frac{I}{I_{mpi}}\right)^n = \left[\frac{\sqrt{\left(f+\frac{2V}{r}\right)\left(f+\frac{\partial rV}{r\partial r}\right)|_{rm}}}{\sqrt{\left(f+\frac{2V}{r}\right)\left(f+\frac{\partial rV}{r\partial r}\right)|^{mpi}_{rmpi}}}\right]^n$, H is the height scale of the TC system, I is the inertial stability frequency at the RMW, and I_{mpi} *is* the inertial stability frequency of the mature storm at

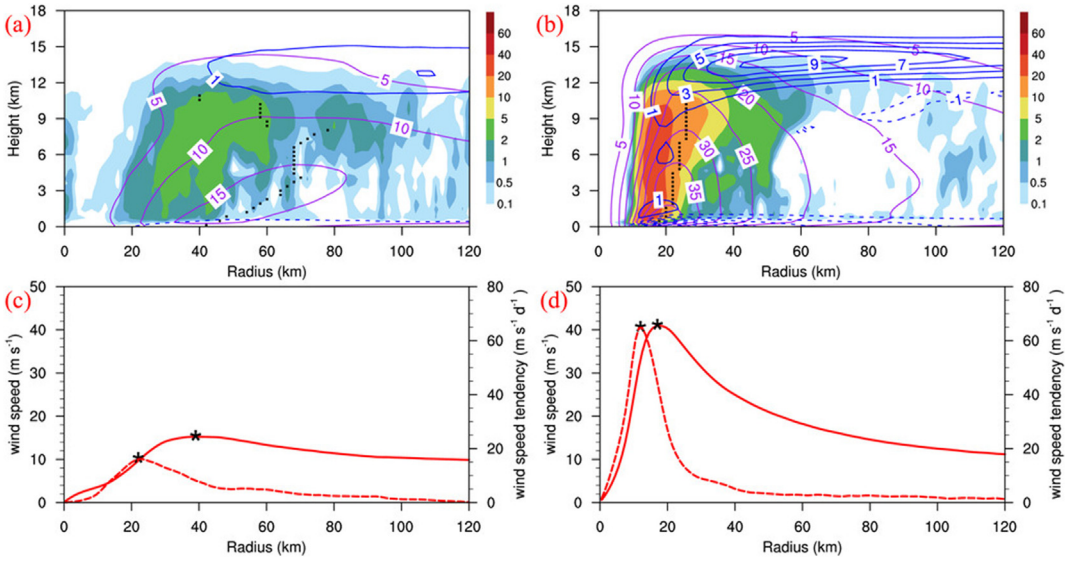

Fig. 8. Results from the idealized simulations of Li et al. (2021): (a, b) Diabatic heating rate (K h^{-1}; shading), tangential wind speed (m s^{-1}; purple), and radial wind speed (m s^{-1}; blue) at the time of (a) the peak RMW contraction rate and (b) the peak intensification rate (IR). The dotted black line denotes the RMW. (c, d) Tangential wind speed (solid) and the tendency of tangential wind speed in the subsequent 6 h (dashed) averaged below 500 m at the time of (c) the peak RMW contraction rate and (d) the peak simulated IR.

its MPI. The weaker the storm, the lower the E value. When a TC approaches its MPI, E is equal to 1.0. By introducing this dynamical efficiency term, the low efficiency in converting latent heating to a TC's kinetic energy during the early development stage is considered, which results in a reasonable prediction of intensity-dependent intensification rate.

Later, in Wang et al. (2021b), the authors introduced, instead of the dynamical efficiency, E, a new *ad-hoc* parameter A, which can be considered as the ventilation parameter, representing the extent of slantwise moist neutrality, which is small for weak TCs and equal to 1.0 as TC reaches slantwise moist neutrality. This is consistent with Peng et al. (2018) that during the early development stage, M and s^* surfaces gradually evolve from almost orthogonal to congruent. Using the tangential wind and entropy budget equations in a slab boundary layer as well as the slantwise moist neutrality scaled by a parameter A, the authors derived an equation similar to (2) above with E replaced by A,

$$\frac{\partial V_m}{\partial \tau} \approx \frac{\alpha C_d}{h}\left(A V_{max}^2 - V_m^2\right), \tag{3}$$

where α is the reduction factor of slab boundary layer wind to the near-surface wind speed; the ventilation parameter A is empirically determined and calibrated using full-physics model simulations and the best-track TC data as $A = (V_m/V_{max})^{3/2}$, which can also share the same expression as the empirically determined E in Wang et al. (2021a). The forecasted relationship between intensification rate and intensity by Equation (3) has a comparable shape to the observed distribution of the 99th percentile of intensification rates (Fig. 9). Promisingly, this modified energetically/dynamically based time-dependent theory can quantitatively capture the intensity dependence of potential intensification rate (PIR) of real TCs as recently evaluated using the best-track TC data for the North Atlantic, eastern and western North Pacific by Xu and Wang (2022).

Equation (3) is then further updated by Wang et al. (2022) including the effect of dissipative heating. $V_{\max}$ in A is reintroduced as a time dependent V_{maxt}, which has a dissipative heating term. With the addition of dissipative heating, the theory predicts not only a shift of the maximum PIR towards the higher intensity side but also higher intensification rate for intense TCs.

Since the current time-dependent theory is highly idealized and does not include any unfavorable environmental effects, such as the large-scale environmental VWS, the theory provides an upper limit of TC intensification rate, or PIR. As mentioned in Wang et al. (2021a, b), hostile environmental factors may reduce the dynamical efficiency (E) or increase the ventilation (reducing the ventilation parameter A) and, thus, these factors need to be included in the time-dependent theory by well-validated parameterizations based on both full-physics numerical simulations and observations such that the theory may be potentially useful for TC intensity forecasts.

3.2. Predictability issues with internal intensity change

Predictability studies are often motivated by spectacular failures of operational forecast models. One striking example was the operational models' failure to anticipate the extreme RI of Hurricane Patricia of 2015—a failure that is particularly vexing because Patricia was found to have high intrinsic predictability (Fox and Judt 2018).

Nystrom and Zhang (2019) showed that model forecasts of Patricia could be much improved by assimilating aircraft radar observations, but they also found that uncertainty in C_k and C_d played a large role in model forecasts missing Patricia's RI. In fact, for very intense storms with high intrinsic predictability

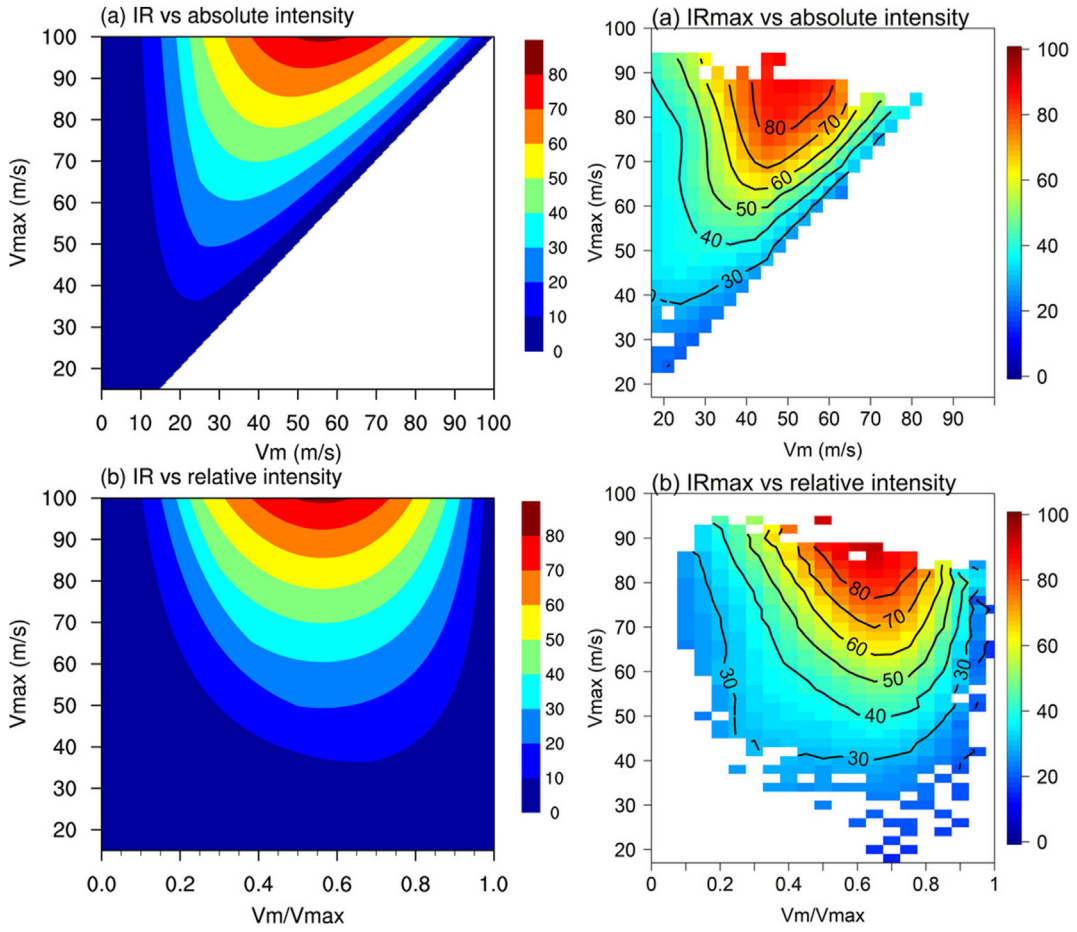

Fig. 9. Left column: Distribution of intensification rates (m s^{-1} day^{-1}) as a function of (top) TC intensity (V_m) and MPI (V_{max}), and (bottom) relative TC intensity (V_m/V_{max}) and V_{max} calculated using Equation (3). Right column: Distribution of the 99th percentile of intensification rates as a function of (top) V_m *and* V_{max}, and (bottom) V_m/V_{max} and V_{max}, using the 6-hourly maximum 10-m sustained wind speed based on the best-track data of TCs in SHIPS (Knaff et al. 2005). Adapted from Figs. 2 and 5 in Wang et al. (2021b).

like Patricia, C_k/C_d uncertainty could be the most important aspect of uncertainty, and a reduction in uncertainty from currently ~40%–1% would be necessary to reduce the ensemble spread to a magnitude that would be produced by small random perturbations (Nystrom and Judt 2022). In further ensemble experiments with Patricia, Nystrom et al. (2020) found that the magnitude of ocean cooling increases with storm intensity and C_d. Additionally, the simulated maximum wind speed uncertainty does not necessarily decrease when ocean feedback is considered.

Tao et al. (2022) used an ensemble of Hurricane Patricia (2015) simulations to distinguish two intensity forecast error sources from vortex structure. Without many hostile impacts from the environment, the limited predictability of Patricia's forecasted intensity is from either a shifted vortex development such that the TC evolves on the same development pathway but shifted in time, or a totally different storm such that there is no moment in time the simulated storm can capture a correct TC structure no matter how it evolves. Given that Patricia has high intrinsic predictability (Fox and Judt 2018), the large forecast errors mainly come from the practical predictability regime, which can be greatly reduced by improving the initial conditions using better data assimilation methods and more inner-core observations in TCs like Patricia.

Many other studies also investigated TC predictability issues caused by the uncertainties in initial inner-core conditions. Nystrom et al. (2018) found that the intensity forecast spread at the early forecast times is mostly determined by the initial errors inside the inner-core region with very little impact from the environment. Similarly, Xu et al. (2022) and Liu et al. (2018) showed that the initial errors from the primary circulation and moisture field inside a TC's inner core can lead to large uncertainties in intensity forecasts. The primary circulation uncertainty directly impacts the boundary layer convergence of angular momentum toward the center and hence the following intensification. The inner-core moisture difference affects the inner-core convective activity immediately, which later influences TC structure and intensification.

The complex multi-scale processes driving TC intensification also motivated efforts of developing a scale-specific stochastic model to examine the cross-scale energy transferring that affects the predictability of TC intensity change (Prasanth et al. 2019). Results in Prasanth et al. (2019) suggest that probabilities of episodic tipping of a TC vortex in response to

an ensemble of stochastic forcings at different scales can potentially produce physically-based intensity forecasts.

Previous studies have shown that TC predictability is both intrinsically and practically limited under vertical wind shear conditions. However, Rios-Berrios (2020) found that extra constraints from radiation can significantly reduce the spread of RI onset times for sheared TCs. This spread reduction is caused by the reduced variability in nonlinear feedbacks among lower-tropospheric ventilation, cold pools, convection, and vortex tilt after turning on the radiation schemes.

Kieu and Rotunno (2022) extended previous work on TC intensity predictability that borrowed from classical predictability theory, i.e., error growth and saturation in spectral space. They concluded that this method has limitations because TC turbulence is not isotropic and homogeneous (an assumption made in classical predictability theory), and possesses different predictability properties from classical turbulence.

In summary, predictability issues arise from model errors (especially uncertainty in C_k and C_d) and initial condition errors (especially inner core structure). While the intrinsic predictability of the atmosphere sets an upper bound for prediction, the practical predictability of TCs can be improved by further reducing model errors and improving the initial conditions.

4. Conclusions

This paper overviews the most significant progress made over 2018–2022 in topic areas related to internal tropical cyclone (TC) intensity change processes. These topics include surface and boundary layer processes, TC internal structure and microphysical processes, and radiation interactions with TCs. Recent studies better frame the uncertainty in the surface drag (C_d) and enthalpy (C_k) coefficients at high wind speeds. Specifically, inconsistency of C_d values at high-wind speeds was found attributable to a few factors: 1) C_d is a function of Reynolds number and wave age rather than the often assumed 10-m wind speed; 2) C_d depends heavily on the sea state; and, 3) there are limitations to the applicability and accuracy of the flux-profile method of C_d estimation at hurricane-force wind speeds using dropsonde data from reconnaissance aircraft. These coefficients greatly impact TC intensity and predictability and it is therefore important that more direct measurements of these surface-layer coefficients are made. Particularly significant scientific strides have been made in TC planetary boundary layers. These advancements have been achieved through improved coupled models, large-eddy simulations, theoretical advancements, and detailed observations including the usage of unmanned aircraft systems. It is now clear that the research field needs to better represent the eddy viscosity throughout the depth of the boundary layer as well as in the eyewall clouds. Furthermore, detailed study of different types of coherent structures in TC PBL will likely be a profitable direction for the research community. Meanwhile, in-depth observational field campaigns and data analysis have made significant headway into verifying theory and modeling studies of intensification processes related to TC vortex alignment, efficient latent heating distributions, and overall 3D structure. An "unusual" vortex alignment pathway through forming a new center downshear of the weak TCs (downshear reformation) was highlighted in recent observational and numerical simulations. Finally, significant effort has been made to better understand the intricate roles radiative processes play in TC evolution and intensity change.

Overall, there have been well-earned gains in the understanding of intensity change processes intrinsic to the TC system. This review focused on recent advances in our understanding of internal mechanisms within a TC that alter a storm's maximum wind speed, but we must emphasize that the internal dynamics related to intensity change are interconnected with the TC's environment and the internal structure of the TC as well. The predictability of intensity changes will continue to improve as our unified understanding of TC multi-scale dynamics advances.

Acknowledgments

We are grateful to all the members of the internal influences of TC intensity change working group for reviewing and documenting the relevant research and operational advances on TC intensity change from 2018–2022. J. Knaff would like to thank the leadership of NOAA's Center for Satellite Applications for their support of this activity. The scientific results and conclusions, as well as any views or opinions expressed herein, are those of the author(s) and do not necessarily reflect those of NOAA or the US Department of Commerce.

References

Ahern, K., Hart, R.E., Bourassa, M.A., 2021. Asymmetric hurricane boundary layer structure during storm decay. Part I: formation of descending inflow. Mon. Wea. Rev. 149, 3851–3874.

Ahern, K., Bourassa, M.A., Hart, R.E., Zhang, J.A., Rogers, R.F., 2019. Observed kinematic and thermodynamic structure in the hurricane boundary layer during intensity change. Mon. Wea. Rev. 147, 2765–2785.

Alford, A.A., Zhang, J.A., Biggerstaff, M.I., Dodge, P., Marks, F.D., Bodine, D.J., 2020. Transition of the hurricane boundary layer during the landfall of Hurricane Irene (2011). J. Atmos. Sci. 77, 3509–3531.

Alland, J.J., Tang, B.H., Corbosiero, K.L., Bryan, G.H., 2021a. Combined effects of midlevel dry air and vertical wind shear on tropical cyclone development. Part I: downdraft ventilation. J. Atmos. Sci. 78, 763–782.

Alland, J.J., Tang, B.H., Corbosiero, K.L., Bryan, G.H., 2021b. Combined effects of midlevel dry air and vertical wind shear on tropical cyclone development. Part II: radial ventilation. J. Atmos. Sci. 78, 783–796.

Alvey, G.R., Fischer, M., Reasor, P., Zawislak, J., Rogers, R., 2022. Observed processes underlying the favorable vortex repositioning early in the development of Hurricane Dorian (2019). Mon. Wea. Rev. 150, 193–213.

Alvey III, G.R., Zipser, E., Zawislak, J., 2020. How does Hurricane Edouard (2014) evolve toward symmetry before rapid intensification? A high-resolution ensemble study. J. Atmos. Sci. 77, 1329–1351.

Bell, M.M., Montgomery, M.T., 2019. Mesoscale processes during the genesis of hurricane Karl (2010). J. Atmos. Sci. 76, 2235–2255.

Carstens, J., Wing, A., 2020. Tropical cyclogenesis from self-aggregated convection in numerical simulations of rotating radiative-convective equilibrium. J. Adv. Model. Earth Syst. 12, e2019MS002020.

Carstens, J.D., Wing, A.A., 2022. A spectrum for convective self-aggregation based on background rotation. J. Adv. Model. Earth Syst. 14, 32021MS002860.

Cha, T.-Y., Bell, M.M., Lee, W.-C., DesRosiers, A.J., 2020. Polygonal eyewall asymmetries during the rapid intensification of Hurricane Michael (2018). Geophys. Res. Letts. 47, e2020GL087919.

Chen, J., Chavas, D.R., 2020. The transient responses of an axisymmetric tropical cyclone to instantaneous surface roughening and drying. J. Atmos. Sci. 77, 2807–2834.

Chen, J., Chavas, D.R., 2021. Can existing theory predict the response of tropical cyclone intensity to idealized landfall? J. Atmos. Sci. 78, 3281–3296.

Chen, X.Y., Ginis, I., Hara, T., 2020. Impact of shoaling ocean surface waves on wind stress and drag coefficient in coastal waters: 2. Tropical cyclones. J. Geophys. Res. 125, e2020JC016223.

Chen, X., Xue, M., Fang, J., 2018a. Rapid intensification of Typhoon Mujigae (2015) under different sea surface temperatures: structural changes leading to rapid intensification. J. Atmos. Sci. 75, 4313–4335.

Chen, X., Wang, Y., Fang, J., Xue, M., 2018b. A numerical study on rapid intensification of Typhoon Vicente (2012) in the south China sea. Part II: roles of inner-core processes. J. Atmos. Sci. 75, 235–255.

Chen, X., Zhang, J.A., Marks, F.D., 2019. A thermodynamic pathway leading to rapid intensification of tropical cyclones in shear. Geophys. Res. Lett. 46, 9241–9251.

Chen, X., Bryan, G.H., 2021. Role of advection of parameterized turbulence kinetic energy in idealized tropical cyclone simulations. J. Atmos. Sci. 78, 3559–3574.

Chen, X., Gu, J.-F., Zhang, J.A., Marks, F.D., Rogers, R.F., Cione, J.J., 2021. Boundary layer recovery and precipitation symmetrization preceding rapid intensification of tropical cyclones under shear. J. Atmos. Sci. 78, 1523–1544.

Chen, X., Bryan, G.H., Zhang, J.A., Cione, J.J., Marks, F.D., 2021a. A framework for simulating the tropical-cyclone boundary layer using large-eddy simulation and its use in evaluating PBL parameterizations. J. Atmos. Sci. 78, 3593–3611.

Chen, X., Xue, M., Zhou, B., Fang, J., Zhang, J.A., Marks, F.D., 2021b. Effect of scale-aware planetary boundary layer schemes on tropical cyclone intensification and structural changes in the gray zone. Mon. Wea. Rev. 149, 2079–2095.

Chen, X., 2022. How do planetary boundary layer schemes perform in hurricane conditions: a comparison with large-eddy simulations. J. Adv. Model. Earth Syst. 14, e2022MS003088.

Chen, X., Bryan, G.H., Hazelton, A., Marks, F.D., Fitzpatrick, P., 2022. Evaluation and improvement of a TKE-based eddy-diffusivity mass-flux (EDMF) planetary boundary layer scheme in hurricane conditions. Wea. Forecast. 37, 935–951.

Cione, J.J., Coauthors, 2020. Eye of the storm: observing hurricanes with a small unmanned aircraft system. Bull. Am. Meteorol. Soc. 101, E186–E205.

Curcic, M., Haus, B.K., 2020. Revised estimates of ocean surface drag in strong winds. Geophys. Res. Lett. 47, e2020GL087647.

Dai, Y., Majumdar, S.J., Nolan, D.S., 2019. The outflow–rainband relationship induced by environmental flow around tropical cyclones. J. Atmos. Sci. 76, 1845–1863.

DeHart, J.C., Bell, M.M., 2020. A comparison of the polarimetric radar characteristics of heavy rainfall from hurricanes Harvey (2017) and Florence (2018). J. Geophys. Res. Atmos. 125, e2019JD032212.

DesRosiers, A.J., Bell, M.M., Cha, T., 2022. Vertical vortex development in Hurricane Michael (2018) during rapid intensification. Mon. Wea. Rev. 150, 99–114.

Didlake Jr., A.C., Houze Jr., R.A., 2013. Dynamics of the stratiform sector of a tropical cyclone rainband. J. Atmos. Sci. 70, 1891–1911.

Didlake Jr., A.C., Reasor, P.D., Rogers, R.F., Lee, W.-C., 2018. Dynamics of the transition from spiral rainbands to a secondary eyewall in Hurricane Earl (2010). J. Atmos. Sci. 75, 2909–2929.

Didlake Jr., A.C., Kumjian, M.R., 2018. Examining storm asymmetries in Hurricane Irma (2017) using polarimetric radar observations. Geophys. Res. Lett. 45, 513–522.

Ditchek, S.D., Molinari, J., Corbosiero, K.L., Fovell, R.G., 2019a. An objective climatology of tropical cyclone diurnal pulses in the Atlantic basin. Mon. Wea. Rev. 147, 591–605.

Ditchek, S.D., Corbosiero, K.L., Fovell, R.G., Molinari, J., 2019b. Electrically active tropical cyclone diurnal pulses in the Atlantic basin. Mon. Wea. Rev. 147, 3595–3607.

Ditchek, S.D., Corbosiero, K.L., Fovell, R.G., Molinari, J., 2020. Electrically active diurnal pulses in Hurricane Harvey (2017). Mon. Wea. Rev. 148, 2283–2305.

Donelan, M.A., 2018. On the decrease of the oceanic drag coefficient in high winds. J. Geophys. Res. 123, 1485–1501.

Dougherty, E.M., Molinari, J., Rogers, R.F., Zhang, J.A., Kossin, J.P., 2018. Hurricane Bonnie (1998): maintaining intensity during high vertical wind shear and an eyewall replacement cycle. Mon. Wea. Rev. 146, 3383–3399.

Dunion, J., Thorncroft, C., Velden, C., 2014. The tropical cyclone diurnal cycle in mature Hurricanes. Mon Wea. Rev. 142, 3900–3919.

Dunion, J., Thorncroft, C., Nolan, D., 2019. Tropical cyclone diurnal cycle signals in a hurricane nature run. Mon Wea. Rev. 147, 363–388.

Duran, E.L., Berndt, E.B., Duran, P., 2021. Observation of the tropical cyclone diurnal cycle using hyperspectral infrared satellite sounding retrievals. Mon. Wea. Rev. 149, 3671–3690.

Emanuel, K.A., 2012. Self-stratification of tropical cyclone outflow: Part II: implications to storm intensification. J. Atmos. Sci. 69, 988–996.

Emanuel, K., 2017. Will global warming make hurricane forecasting more difficult? Bull. Am. Meteorol. Soc. 98, 495–501.

Evans, R., Nolan, D., 2019. Balanced and radiating wave responses to diurnal heating in tropical cyclone-like vortices using a linear non-hydrostatic model. J. Atmos. Sci. 76, 2575–2597.

Evans, R., Nolan, D., 2022. The spatiotemporal evolution of the diurnal cycle in two WRF simulations of tropical cyclones. J. Atmos. Sci. 79, 1021–1043.

Fei, R., Wang, Y., Li, Y., 2021. Contribution of vertical advection to super-gradient wind in tropical cyclone boundary layer: a numerical study. J. Atmos. Sci. 78, 1057–1073.

Feng, Y.-C., Bell, M.M., 2018. Microphysical characteristics of an asymmetric eyewall in major Hurricane Harvey (2017). Geophys. Res. Lett. https://doi.org/10.1029/2018gl080770.

Fischer, M.S., Rogers, R.F., Reasor, P.D., 2020. The rapid intensification and eyewall replacement cycles of Hurricane Irma (2017). Mon. Wea. Rev. 148, 981–1004.

Fischer, M.S., Reasor, P.D., Rogers, R.F., Gamache, J.F., 2022. An analysis of tropical cyclone vortex and convective characteristics in relation to storm intensity using a novel airborne Doppler radar database. Mon. Wea. Rev. 150, 2255–2278.

Fox, K.R., Judt, F., 2018. A numerical study on the extreme intensification of Hurricane Patricia (2015). Wea. Forecast. 33, 989–999.

Gao, K., Ginis, I., 2018. On the characteristics of linear-phase roll vortices under a moving hurricane boundary layer. J. Atmos. Sci. 75, 2589–2598.

Gopalakrishnan, S., Hazelton, A., Zhang, J.A., 2021. Improving hurricane boundary layer parameterization scheme based on observations. Earth Space Sci. 8, e2020EA001422.

Gu, J.-F., Tan, Z.-M., Qiu, X., 2018. The evolution of vortex tilt and vertical motion of tropical cyclones in directional shear flows. J. Atmos. Sci. 75, 3565–3578.

Gu, J.-F., Tan, Z.-M., Qiu, X., 2019. Intensification variability of tropical cyclones in directional shear flows: vortex tilt–convection coupling. J. Atmos. Sci. 76, 1827–1844.

Guimond, S.R., Zhang, J.A., Sapp, J.W., Frasier, S.J., 2018. Coherent turbulence in the boundary layer of Hurricane Rita (2005) during an eyewall replacement cycle. J. Atmos. Sci. 75, 3071–3093.

Guo, X., Tan, Z.-M., 2017. Tropical cyclone fullness: a new concept for interpreting storm intensity. Geophys. Res. Letts. 44, 4324–4331.

Guo, X., Tan, Z.-M., 2022. Tropical cyclone intensification and fullness: the role of storm size configuration. Geophys. Res. Lett. 49, e2022GL098449.

Hazelton, A., Zhang, J.A., Gopalakrishnan, S., 2022. Comparison of the performance of the observation-based hybrid EDMF and EDMF-TKE PBL schemes in 2020 tropical cyclone forecasts from the global-nested Hurricane Analysis and Forecast System. Wea. Forecast. 37, 457–476.

He, J.Y., Chan, P.W., Li, Q.S., Li, L., Zhang, L., Yang, H.L., 2022. Observations of wind and turbulence structures of Super Typhoons Hato and Mangkhut over land from a 356 m high meteorological tower. Atmos. Res. 265, 105910.

Hendricks, E.A., Knievel, J.C., Nolan, D.S., 2021. Evaluation of boundary layer and urban canopy parameterizations for simulating wind in Miami during Hurricane Irma (2017). Mon. Wea. Rev. 149, 2321–2349.
Hlywiak, J., Nolan, D.S., 2021. The response of the near-surface tropical cyclone wind field to inland surface roughness length and soil moisture content during and after landfall. J. Atmos. Sci. 78, 983–1000.
Hlywiak, J., Nolan, D.S., 2022. The evolution of asymmetries in the tropical cyclone boundary layer wind field during landfall. Mon. Wea. Rev. 150, 529–549.
Holthuijsen, L.H., Powell, M.D., Pietrzak, J.D., 2012. Wind and waves in extreme hurricanes. J. Geophys. Res. 117.
Homeyer, C.R., Coauthors, 2021. Polarimetric signatures in landfalling tropical cyclones. Mon. Wea. Rev. 149, 131–154.
Hu, C., Wu, C., 2020. Ensemble sensitivity analysis of tropical cyclone intensification rate during the development stage. J. Atmos. Sci. 77, 3387–3405.
Huang, H., Coauthors, 2022a. Microphysical characteristics of the phase-locking VRW-induced asymmetric convection in the outer eyewall of Super Typhoon Lekima (2019). Geophys. Res. Lett. 49, e2021GL096869.
Huang, H., Coauthors, 2022b. Turbulent fluxes and surface meteorology during the landfall of four typhoons in the South China Sea. Mon. Wea. Rev. 150, 1799–1831.
Jarosz, E., Mitchell, D.A., Wang, D.W., Teague, W.J., 2007. Bottom-up determination of air-sea momentum exchange under a major tropical cyclone. Science 315, 1707–1709.
Jiang, J., Wang, Y., 2022. The roles of barotropic instability and the beta effect in the eyewall evolution of tropical cyclones. Adv. Atmos. Sci. 39, 1800–1815.
Kalina, E.A., Biswas, M.K., Zhang, J.A., Newman, K.M., 2021. Sensitivity of an idealized tropical cyclone to the configuration of the Global Forecast System–Eddy Diffusivity Mass Flux planetary boundary layer scheme. Atmosphere 12, 284.
Kaplan, J., DeMaria, M., Knaff, J.A., 2010. A revised tropical cyclone rapid intensification for the Atlantic and eastern North Pacific basins. Wea. Forecast. 25, 220–241.
Kieu, C., Rotunno, R., Wang, Q., 2020. Frictionally induced feedback in a reduced dynamical model of tropical cyclone intensification. J. Atmos. Sci. 77, 3821–3831.
Kieu, C., Rotunno, R., 2022. Characteristics of tropical cyclone turbulence and intensity predictability. Geophys. Res. Letts. 49, e2021GL096544.
Kim, S.-H., Kang, H.-W., Moon, I.-J., Kang, S.K., Chu, P.-S., 2022. Effects of the reduced air-sea drag coefficient in high winds on the rapid intensification of tropical cyclones and bimodality of the lifetime maximum intensity. Front. Mar. Sci. 9.
Knaff, J.A., Sampson, C.R., DeMaria, M., 2005. An operational statistical typhoon intensity prediction scheme for the western North Pacific. Wea. Forecast. 20, 688–699.
Knaff, J., Slocum, C., Musgrave, K., 2019. Quantification and exploration of diurnal oscillations in tropical cyclones. Mon. Wea. Rev. 142, 2105–2121.
Komori, S., Iwano, K., Takagaki, N., Onishi, R., Kurose, R., Takahashi, K., Suzuki, N., 2018. Laboratory measurements of heat transfer and drag coefficients at extremely high wind speeds. J. Phys. Oceanogr. 48, 959–974.
Kudryavtsev, V., Monzikova, A., Combot, C., Chapron, B., Reul, N., Quilfen, Y., 2019a. A simplified model for the baroclinic and barotropic ocean response to moving tropical cyclones: 1. Satellite observations. J. Geophys. Res. Oceans 124, 3446–3461.
Kudryavtsev, V., Monzikova, A., Combot, C., Chapron, B., Reul, N., 2019b. A simplified model for the baroclinic and barotropic ocean response to moving tropical cyclones: 2. Model and simulations. J. Geophys. Res.-Oceans 124, 3462–3485.
Kuo, H.-C., Tsujino, S., Hsu, T.-Y., Peng, M.S., Su, S.-H., 2022. Scaling law for boundary layer inner eyewall pumping in concentric eyewalls. J. Geophys. Res.-Atmos. 127, e2021JD035518.
Lai, T.-K., Menelaou, K., Yau, M.K., 2019. Barotropic instability across the moat and inner eyewall dissipation: a numerical study of Hurricane Wilma (2005). J. Atmos. Sci. 76, 989–103.
Lai, T.-K., Hendricks, E.A., Yau, M.K., Menelaou, K., 2021a. Roles of barotropic instability across the moat in Inner eyewall decay and outer eyewall intensification: three-dimensional numerical experiments. J. Atmos. Sci. 78, 473–496.
Lai, T.-K., Hendricks, E.A., Yau, M.K., Menelaou, K., 2021b. Roles of barotropic instability across the moat in inner eyewall decay and outer eyewall intensification: essential dynamics. J. Atmos. Sci. 78, 1411–1428.
Lai, T.-K., Hendricks, E.A., Yau, M.K., 2021c. Long-term effect of the barotropic instability across the moat on double-eyewall tropical cyclone-like vortices in forced and unforced shallow water models. J. Atmos. Sci. 78, 4103–4126.
Lee, J.-D., Wu, C.-C., Ito, K., 2020. Diurnal variation of the convective area and eye size associated with the rapid intensification of tropical cyclones. Mon. Wea. Rev. 143, 4061–4082.
Li, T.-H., Wang, Y., 2021a. The role of boundary layer dynamics in tropical cyclone intensification. Part I: sensitivity to surface drag coefficient. J. Meteorol. Soc. Jpn. 99, 537–554.
Li, T.-H., Wang, Y., 2021b. The role of boundary layer dynamics in tropical cyclone intensification. Part II: sensitivity to initial vortex structure. J. Meteorol. Soc. Jpn. 99, 555–573.
Li, X., Pu, Z., 2021. Vertical eddy diffusivity parameterization based on a large-eddy simulation and its impact on prediction of hurricane landfall. Geophys. Res. Lett. 48, e2020GL090703.
Li, X., Cheng, X., Fei, J., Huang, X., Ding, J., 2022a. The modulation effect of sea surface cooling on the eyewall replacement cycle in Typhoon Trami (2018). Mon. Wea. Rev. 150, 1417–1436.
Li, Y., Wang, Y., Lin, Y., 2019. Revisiting the dynamics of eyewall contraction of tropical cyclones. J. Atmos. Sci. 76, 3229–3245.
Li, Y., Wang, Y., Lin, Y., 2020. How much does the upward advection of the supergradient component of boundary layer wind contribute to tropical cyclone intensification and maximum intensity? J. Atmos. Sci. 77, 2649–2664.
Li, Y.-L., Wang, Y., Lin, Y.-L., Wang, X., 2021. Why does rapid contraction of the radius of maximum wind precede rapid intensification in tropical cyclones? J. Atmos. Sci. 78, 3441–3453.
Li, Y., Wang, Y., Tan, Z.-M., 2022b. Why does the initial wind profile inside the radius of maximum wind matter to tropical cyclone development. J. Geophys. Res. Atmos. 127, e2022JD037039.
Li, Y.-L., Wang, Y., Tan, Z.-M., 2022c. How frequently does rapid intensification occur after rapid contraction of the radius of maximum wind in tropical cyclones over the North Atlantic and Eastern North Pacific? Mon. Wea. Rev. 150, 1747–1760.
Li, Y.-L., Tan, Z.-M., Wang, Y., 2022d. Relative timing of the ends of hurricane intensification and contraction of the radius of maximum wind in the North Atlantic and Eastern North Pacific. Geophys. Res. Lett. 49, e2022GL101027.
Liu, H.-Y., Wang, Yuqing, Gu, J.-F., 2021. Intensity change of binary tropical cyclones (TCs) in idealized numerical simulations: two initially identical mature TCs. J. Atmos. Sci. 78, 1001–1020.
Liu, S., Tao, D., Zhao, K., Minamide, M., Zhang, F., 2018. Dynamics and predictability of the rapid intensification of super typhoon usagi (2013). J. Geophys. Res. Atmos. 123, 7462–7481.
Mashiko, W., Shimada, S., 2021. Observed near-surface wind structure in the inner core of Typhoon Goni (2015). Mon. Wea. Rev. 149, 1785–1800.
Miyamoto, Y., Nolan, D.S., 2018. Structural changes preceding rapid intensification in tropical cyclones as shown in a large ensemble of idealized simulations. J. Atmos. Sci. 75, 555–569.
Moon, Y., Nolan, D.S., 2010. The dynamic response of the hurricane wind field to spiral rainband heating. J. Atmos. Sci. 67, 1779–1805.
Muller, C.J., Romps, D.M., 2018. Acceleration of tropical cyclogenesis by self-aggregation feedbacks. Proc. Nat. Acad. Sci. 115, 2930–2935.
Nam, C.C., Bell, M.M., 2021. Multiscale shear impacts during the genesis of Hagupit (2008). Mon. Wea. Rev. 149, 551–569.
Nguyen, L.T., Rogers, R., Zawislak, J., Zhang, J.A., 2019. Assessing the influence of convective downdrafts and surface enthalpy fluxes on tropical cyclone intensity change in moderate vertical wind shear. Mon. Wea. Rev. 147, 3519–3534.
Nolan, D.S., McNoldy, B.D., Ge, J.Y., 2021a. Evaluation of the surface wind field over land in WRF simulations of Hurricane Wilma (2005). Part I: model initialization and simulation validation. Mon. Wea. Rev. 149, 679–695.
Nolan, D.S., McNoldy, B.D., Ge, J.Y., 2021b. Evaluation of the surface wind field over land in WRF simulations of Hurricane Wilma (2005). Part II:

surface winds, inflow angles, and boundary layer profiles. Mon. Wea. Rev. 149, 697–713.
Nystrom, R.G., Zhang, F., Munsell, E.B., Braun, S., Sippel, J.A., Weng, Y., Emanuel, K., 2018. Predictability and dynamics of Hurricane Joaquin (2015) explored through convection-permitting ensemble sensitivity experiments. J. Atmos. Sci. 75, 401–424.
Nystrom, R.G., Zhang, F., 2019. Practical uncertainties in the limited predictability of the record-breaking intensification of Hurricane Patricia (2015). Mon. Wea. Rev. 147, 3535–3556.
Nystrom, R.G., Chen, X., Zhang, F., Davis, C.A., 2020a. Nonlinear impacts of surface exchange coefficient uncertainty on tropical cyclone intensity and air-sea interactions. Geophys. Res. Letts. 47, e2019GL085783.
Nystrom, R.G., Rotunno, R., Davis, C.A., Zhang, F., 2020b. Consistent impacts of surface enthalpy and drag coefficient uncertainty between an analytical model and simulated tropical cyclone maximum intensity and storm structure. J. Atmos. Sci. 77, 3059–3080.
Nystrom, R.G., Judt, F., 2022. The consequences of surface-exchange coefficient uncertainty on an otherwise highly predictable major hurricane. Mon. Wea. Rev. 150, 2073–2089.
Park, J., Cha, D.-H., Lee, M.-K., Moon, J., Hahm, S.-J., Noh, K., Chan, J., Bell, M.M., 2020. Impact of cloud microphysics schemes on tropical cyclone forecast over the western North Pacific. J. Geophys. Res. Atmos. 125, e2019JD032288.
Peng, C.-H., Wu, C.-C., 2020. The impact of outer-core surface heat fluxes on the convective activities and rapid intensification of tropical cyclones. J. Atmos. Sci. 77, 3907–3927.
Peng, K., Rotunno, R., Bryan, G.H., 2018. Evaluation of a time- dependent model for the intensification of tropical cyclones. J. Atmos. Sci. 75, 2125–2138.
Peng, K., Rotunno, R., Bryan, G.H., Fang, J., 2019. Evolution of an axisymmetric tropical cyclone before reaching slantwise moist neutrality. J. Atmos. Sci. 76, 1865–1884.
Peng, K., Fang, J., 2021. Effect of the initial vortex vertical structure on early development of an axisymmetric tropical cyclone. J. Geophys. Res. Atmos. 126, e2020JD033697.
Prasanth, S., Rao, P.S.C., Marks Jr., F.D., 2019. A conceptual framework for the scale-specific stochastic modeling of transitions in tropical cyclone intensities. Earth Space Sci. 6, 972–981.
Qin, N., Zhang, D.-L., Li, Y., 2016. A statistical analysis of steady eyewall sizes associated with rapidly intensifying hurricanes. Wea. Forecast. 31, 737–743.
Raymond, D.J., Gjorgjievska, S., Sessions, S., Fuchs, Z., 2014. Tropical cyclogenesis and mid-level vorticity. Aust. Meteorol. Oceanogr. J. 64, 11–25.
Raymond, D.J., Flores, M.M., 2016. Predicting convective rainfall over tropical oceans from environmental conditions. J. Adv. Model. Earth Syst. 8, 703–718.
Raymond, D.J., Kilroy, G., 2019. Control of convection in high-resolution simulations of tropical cyclogenesis. J. Adv. Model. Earth Syst. 11, 1582–1599.
Raymond, D.J., Fuchs-Stone, Z., 2021. Emergent properties of convection in OTREC and PREDICT. J. Geophys. Res. Atmos. 126, e2020JD033585.
Richter, D.H., Wainwright, C., Stern, D.P., Bryan, G.H., Chavas, D., 2021. Potential low bias in high-wind drag coefficient inferred from dropsonde data in hurricanes. J. Atmos. Sci. 78, 2339–2352.
Riemer, M., Montgomery, M.T., Nicholls, M.E., 2010. A new paradigm for intensity modification of tropical cyclones: thermodynamic impact of vertical wind shear on the inflow layer. Atmos. Chem. Phys. 10, 3163–3188.
Rios-Berrios, R., Davis, C.A., Torn, R.D., 2018. A hypothesis for the intensification of tropical cyclones under moderate vertical wind shear. J. Atmos. Sci. 75, 4149–4173.
Rios-Berrios, R., 2020. Impacts of radiation and cold pools on the intensity and vortex tilt of weak tropical cyclones interacting with vertical wind shear. J. Atmos. Sci. 77, 669–689.
Rogers, R.F., Reasor, P.D., Zawislak, J.A., Nguyen, L.T., 2020. Precipitation processes and vortex alignment during the intensification of a weak tropical cyclone in moderate vertical shear. Mon. Wea. Rev. 148, 1899–1929.
Ruppert, J., O'Neill, M., 2019. Diurnal cloud and circulation changes in simulated tropical cyclones. Geophys. Res. Letts. 46, 502–511.
Ruppert, J., Wing, A., Tang, X., Duran, E., 2020. The critical role of cloud-infrared radiation feedback in tropical cyclone development. Proc. Nat. Acad. Sci. 117, 27884–27892.
Ryglicki, D.R., Doyle, J.D., Hodyss, D., Cossuth, J.H., Jin, Y., Viner, K.C., Schmidt, J.M., 2019. The unexpected rapid intensification of tropical cyclones in moderate vertical wind shear. Part III: outflow-environment interaction. Mon. Wea. Rev. 147, 2919–2940.
Schecter, D.A., Menelaou, K., 2020. Development of a misaligned tropical cyclone. J. Atmos. Sci. 77, 79–111.
Schecter, D.A., 2022. Intensification of tilted tropical cyclones over relatively cool and warm oceans in idealized numerical simulations. J. Atmos. Sci. 79, 485–512.
Sentic, S., Sessions, S.L., Fuchs, Z., 2015. Diagnosing DYNAMO convection with weak temperature gradient simulations. J. Adv. Model. Earth Syst. 7, 1849–1871.
Sessions, S.L., Herman, M.J., Sentic, S., 2015. Convective response to changes in the thermodynamic environment in idealized weak temperature gradient simulations. J. Adv. Model. Earth Syst. 7, 712–738.
Smith, R.K., Kilroy, G., Montgomery, M.T., 2021. Tropical cyclone life cycle in a three-dimensional numerical simulation. Quart. J. Roy. Meteorol. Soc. 147, 3373–3393.
Smith, W., Nicholls, M.E., Pielke, R., 2020. The role of radiation in accelerating tropical cyclogenesis in idealized simulations. J. Atmos. Sci. 77, 1261–1277.
Sparks, N., Hon, K.K., Chan, P.W., Wang, S., Chan, J.C.L., Lee, T.C., Toumi, R., 2019. Aircraft observations of tropical cyclone boundary layer turbulence over the South China Sea. J. Atmos. Sci. 76, 3773–3783.
Sroka, S., Guimond, S.R., 2021. Organized kinetic energy backscatter in the hurricane boundary layer from radar measurements. J. Fluid Mech. 924, A21.
Stern, D.P., Vigh, J.L., Nolan, D.S., Zhang, F., 2015. Revisiting the relationship between eyewall contraction and intensification. J. Atmos. Sci. 72, 1283–1306.
Sun, L., Tang, X., Zhuge, X., Tan, Z.-M., Fang, J., 2021. Diurnal variation of overshooting tops in typhoons detected by Himawari-8 satellite. Geophys. Res. Letts. 48, e2021GL095565.
Tang, J., Zhang, J.A., Aberson, S.D., Marks, F.D., Lei, X., 2018. Multilevel tower observations of vertical eddy diffusivity and mixing length in the tropical cyclone boundary layer during landfalls. J. Atmos. Sci. 75, 3159–3168.
Tang, J., Zhang, J.A., Chan, P., Hon, K., Lei, X., Wang, Y., 2021. A direct aircraft observation of helical rolls in the tropical cyclone boundary layer. Scientific Rep. 11, 18771.
Tang, X., Tan, Z.-M., Fang, J., Munsell, E., Zhang, F., 2019. Impact of the diurnal radiation contrast on the contraction of radius of maximum wind during intensification of Hurricane Edouard (2014). J. Atmos. Sci. 76, 421–432.
Tao, D., Zhang, F., 2019. Evolution of dynamic and thermodynamic structures before and during rapid intensification of tropical cyclones: sensitivity to vertical wind shear. Mon. Wea. Rev. 147, 1171–1191.
Tao, D., van Leeuwen, P.J., Bell M, M., Ying, Y., 2022. Dynamics and predictability of tropical cyclone rapid intensification in ensemble simulations of Hurricane Patricia (2015). J. Geophys. Res. Atmos. 127, e2021JD036079.
Trabing, B., Bell, M., Brown, B., 2019. Impacts of radiation and upper-tropospheric temperatures on tropical cyclone structure and intensity. J. Atmos. Sci. 76, 135–153.
Trabing, B.C., Bell, M.M., 2021. The sensitivity of eyewall replacement cycles to shortwave radiation. J. Geophys. Res. 126, e2020JD034016.
Troitskaya, Y., Druzhinin, O., Kozlov, D., Zilitinkevich, S., 2018. The “bag breakup” spume droplet generation mechanism at high winds. Part II: contribution to momentum and enthalpy transfer. J. Phys. Oceanogr. 48, 2189–2207.
Tsai, Y.-S., Miau, J.-J., Yu, C.-M., Chang, W.-T., 2019. Lidar observations of the typhoon boundary layer within the outer rainbands. Bound.-Layer Meteorol. 171, 237–255.
Tsujino, S., Kuo, H.-C., 2020. Potential vorticity mixing and rapid intensification in the numerically simulated Supertyphoon Haiyan (2013). J. Atmos. Sci. 77, 2067–2090.

Vigh, J.L., CoAuthors, 2018. Topic (3.1): intensity change: internal influences. *Ninth International Workshop on Tropical Cyclones (IWTC-9) Report*.

Vaughan, A., Walsh, K.J.E., Kepert, J.D., 2020. The stationary banding complex and secondary eyewall formation in tropical cyclones. J. Geophys. Res.-Atmos. 125, e2019JD031515. https://doi.org/10.1029/2019JD031515.

Wadler, J.B., Zhang, J.A., Rogers, R.F., Jaimes, B., Shay, L.K., 2021. The rapid intensification of Hurricane Michael (2018): storm structure and the relationship to environmental and air–sea interactions. Mon. Wea. Rev. 149, 245–267.

Wadler, J.B., Cione, J.J., Zhang, J.A., Kalina, E.A., Kaplan, J., 2022. The effects of environmental wind shear direction on tropical cyclone boundary layer thermodynamics and intensity change from multiple observational datasets. Mon. Wea. Rev. 150, 115–134.

Wang, H., Wang, Y., Xu, J., Duan, Y.-H., 2019. The axisymmetric and asymmetric aspects of the secondary eyewall formation in a numerically simulated tropical cyclone under idealized conditions on an *f*-plane. J. Atmos. Sci. 76, 357–378.

Wang, X., Jiang, H., 2021. Contrasting behaviors between the rapidly intensifying and slowly intensifying tropical cyclones in the North Atlantic and Eastern Pacific basins. J. Clim. 34, 987–1003.

Wang, Y., Li, Y.-L., Xu, J., Tan, Z.-M., Lin, Y.-L., 2021a. The intensity-dependence of tropical cyclone intensification rate in a simplified energetically based dynamical system model. J. Atmos. Sci. 78, 2033–2045.

Wang, Y., Li, Y.-L., Xu, J., 2021b. A new time-dependent theory of tropical cyclone intensification. J. Atmos. Sci. 78, 3855–3865.

Wang, Y., Xu, J., Tan, Z.-M., 2022. Contribution of dissipative heating to the intensity-dependence of tropical cyclone intensification. J. Atmos. Sci. 79, 2169–2180.

Wang, Y.-F., Tan, Z.-M., 2020. Outer rainbands-driven secondary eyewall formation of tropical cyclones. J. Atmos. Sci. 77, 2217–2236.

Wang, Y.-F., Tan, Z.-M., 2022. Essential dynamics of the vertical wind shear affecting the secondary eyewall formation in tropical cyclones. J. Atmos. Sci. 79, 2831–2847.

Wing, A., Coauthors, 2019. Moist static energy budget analysis of tropical cyclone intensification in high-resolution climate models. J. Clim. 32, 6071–6095.

Wing, A., 2022. Acceleration of tropical cyclone development by cloud-radiative feedbacks. J. Atmos. Sci. 79, 2285–2305.

Wu, D., Coauthors, 2018. Kinematics and microphysics of convection in the outer rainband of Typhoon Nida (2016) revealed by polarimetric radar. Mon. Wea. Rev. 146, 2147–2159.

Wu, D., Coauthors, 2021. Evaluation of microphysics schemes in tropical cyclones using polarimetric radar observations: convective precipitation in an outer rainband. Mon. Wea. Rev. 149, 1055–1068.

Wu, Q., Hong, J., Ruan, Z., 2020. Diurnal variations in tropical cyclone intensification. Geophys. Res. Letts. 47, e2020GL090397.

Wu, Q., Ruan, Z., 2021. Rapid contraction of the radius of maximum tangential wind and rapid intensification of a tropical cyclone. J. Geophys. Res.-Atmos. 126, e2020JD033681.

Wu, Q., Hong, J., 2022. Diurnal variations in contraction of the radius of maximum tangential wind in tropical cyclones. Geophys. Res. Letts. 49, e2021GL096048.

Wu, S.-N., Soden, B.J., Nolan, D.S., 2021. Examining the role of cloud radiative interactions in tropical cyclone development using satellite measurements and WRF simulations. Geophys. Res. Letts. 48, e2021GL093259.

Xu, J., Wang, Y., 2018. Dependence of tropical cyclone intensification rate on sea surface temperature, storm intensity and size in the western North Pacific. Wea. Forecast. 33, 523–537.

Xu, J., Wang, Y., 2022. Potential intensification rate of tropical cyclones in a simplified energetically based dynamical system model: an observational analysis. J. Atmos. Sci. 79, 1045–1055.

Xu, M., Li, H., Luo, J., Ben, H., Zhu, Y., 2022. Predictability and dynamics of the rapid intensification of super typhoon lekima (2019). Front. Earth Sci. 16, 132–143.

Yang, B., Nie, J., Tan, Z.-M., 2021a. Radiation feedback accelerates the formation of Typhoon Haiyan (2013): the critical role of mid-level circulation. Geophys. Res. Lett. 48, e2021GL094168.

Yang, B., Guo, X., Gu, J.-F., Nie, J., 2022. Radiation feedback prevents tropical cyclones from reaching higher intensity. Geophys. Res. Lett. 49, e2022GL100067.

Yang, B., Tan, Z.-M., 2020. Interactive radiation accelerates the intensification of the midlevel vortex for tropical cyclogenesis. J. Atmos. Sci. 77, 4051–4065.

Yang, L., Cheng, X., Huang, X., Fei, J., Li, X., 2019. Effects of air-sea interaction on the eyewall replacement cycle of Typhoon Sinlaku (2008): verification of numerical simulation. Earth Space Sci. 7, e2019EA000763.

Yang, Y.-T., Kuo, H.-C., Tsujino, S., Chen, B.-F., Peng, M.S., 2021b. Characteristics of long-lived concentric eyewalls in tropical cyclones. J. Geophys. Res.-Atmos. 126, e2020JD033703.

Yu, C., Didlake Jr., A.C., 2019. Impact of stratiform rainband heating on the tropical cyclone wind field in idealized simulations. J. Atmos. Sci. 76, 2443–2462.

Yu, C.-L., Didlake, A.C., Zhang, F., Nystrom, R.G., 2021. Asymmetric rainband processes leading to secondary eyewall formation in a model simulation of Hurricane Matthew (2016). J. Atmos. Sci. 78, 29–49.

Zhang, B., Soden, B.J., Vecchi, G.A., Yang, W., 2021. The role of radiative interactions in tropical cyclone development under realistic boundary conditions. J. Clim. 34, 2079–2091.

Zhang, J.A., Marks, F.D., Montgomery, M.T., Lorsolo, S., 2011. An estimation of turbulent characteristics in the low-level region of intense Hurricanes Allen (1980) and Hugo (1989). Mon. Wea. Rev. 139, 1447–1462.

Zhang, J., Dunion, J., Nolan, D., 2020. In situ observations of the diurnal variation in the boundary layer of mature hurricanes. Geophys. Res. Letts. 47, 1–8.

Zhang, X., Xu, W., 2021. Strong diurnal pulsing of cold clouds in rapidly intensifying tropical cyclones. Geophys. Res. Letts. 48, e2021GL094773.

Zhao, Z., Chan, P.W., Wu, N., Zhang, J.A., Hon, K.K., 2020. Aircraft observations of turbulence characteristics in the tropical cyclone boundary layer. Bound.-Layer Meteorol. 174, 493–511.

Zhou, X., Hara, T., Ginis, I., D'Asaro, E., Hsu, J.-Y., Reichl, B.G., 2022. Drag coefficient and its sea state dependence under tropical cyclones. J. Phys. Oceanogr. 52, 1447–1470.

Zhu, P., Hazelton, A., Zhang, Z., Marks, F.D., Tallapragada, V., 2021. The role of eyewall turbulent transport in the pathway to intensification of tropical cyclones. J. Geophys. Res. 126, e2021JD034983.

Zhu, X.-S., Yu, H., Wang, Y., 2022. Downwind development in a stationary band complex leading to the secondary eyewall formation in the simulated Typhoon Soudelor (2015). Mon. Wea. Rev. 150, 2459–2483.